Science of the Total Environment 654 (2019) 1241–1257

Contents lists available at ScienceDirect

Science of the Total Environment

journal homepage: www.elsevier.com/locate/scitotenv

Source apportionment of an epiphytic lichen biomonitor to elucidate the sources and spatial distribution of polycyclic aromatic hydrocarbons in the Athabasca Oil Sands Region, Alberta, Canada

Matthew S. Landis [a,*], William B. Studabaker [b], J. Patrick Pancras [c], Joseph R. Graney [d], Keith Puckett [e], Emily M. White [f], Eric S. Edgerton [g]

[a] Integrated Atmospheric Solutions, LLC, Cary, NC, USA
[b] Tobacco Road Collaborative, LLC, Raleigh, NC, USA
[c] Pancras Consulting, Cary, NC, USA
[d] Geological Sciences and Environmental Studies, Binghamton University, Binghamton, NY, USA
[e] ECOFIN, Waldemar, Ontario, Canada
[f] Maed Consulting, Pittsboro, NC, USA
[g] Atmospheric Research & Analysis, Inc., Cary, NC, USA

HIGHLIGHTS

- Epiphytic lichen PAH bioindicator study conducted in Athabasca Oil Sands Region
- Receptor modeling elucidated and quantified significant contributing sources.
- C1-C2-alkyl PAHs and dibenzothiophenes utilized as tracer species
- Petroleum coke and raw oil sand dust accounted for 67% of near field ΣPAH deposition.
- Petroleum coke source required the use of C1-C2-alkyl PAH tracer species to resolve.

GRAPHICAL ABSTRACT

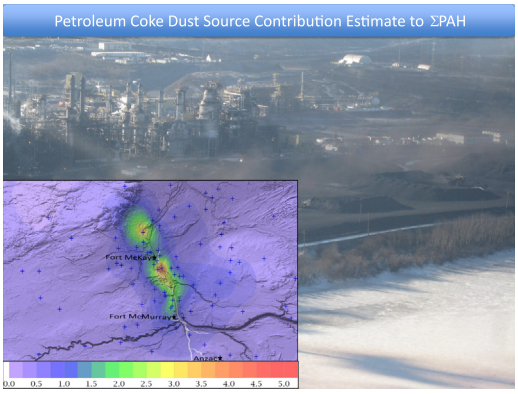

ARTICLE INFO

Article history:
Received 20 July 2018
Received in revised form 28 October 2018
Accepted 9 November 2018
Available online 12 November 2018

Editor: Kelly Roland Munkittrick

Keywords:
Lichen
Hypogymnia physodes
Biomonitor

ABSTRACT

The sources and spatial distribution of polycyclic aromatic hydrocarbons (PAHs) atmospheric deposition in the boreal forests surrounding bitumen production operations in the Athabasca Oil Sands Region (AOSR), Alberta, Canada were investigated as part of a 2014 passive in-situ bioindicator source apportionment study. Epiphytic lichen species *Hypogymnia physodes* samples (n = 127) were collected within a 150 km radius of the main surface oil sand production operations and analyzed for total sulfur, total nitrogen, forty-three elements, twenty-two PAHs, ten groups of C1-C2-alkyl PAHs and dibenzothiophenes (polycyclic aromatic compounds; PACs), five C1- and C2-alkyldibenzothiophenes, and retene. The ΣPAH + PAC in *H. physodes* ranged from 54 to 2778 ng g^{-1} with a median concentration of 317 ng g^{-1}. Source apportionment modeling found an eight-factor solution that explained 99% of the measured ΣPAH + PAC lichen concentrations from four anthropogenic oil sands production sources (Petroleum Coke, Haul Road Dust, Stack Emissions, Raw Oil Sand), two local/regional sources (Biomass Combustion, Mobile Source), and two lichen biogeochemical factors. Petroleum Coke and Raw Oil

* Corresponding author.
E-mail address: mlandis@atmospheric-solutions.com (M.S. Landis).

https://doi.org/10.1016/j.scitotenv.2018.11.131

Polycyclic aromatic compounds
Atmospheric deposition

Sand dust were identified as the major contributing sources of ΣPAH + PAC in the AOSR. These two sources accounted for 63% (43.2 μg g^{-1}) of ΣPAH + PAC deposition to the entire study domain. Of this overall 43.2 μg g^{-1} contribution, approximately 90% (39.9 μg g^{-1}) ΣPAH + PAC was deposited within 25 km of the closest oil sand production facility. Regional sources (Biomass Combustion and Mobile Sources) accounted for 19% of ΣPAH + PAC deposition to the entire study domain, of which 46% was deposited near-field to oil sand production operations. Source identification was improved over a prior lichen-based study in the AOSR through incorporation of PAH and PAC analytes in addition to inorganic analytes.

1. Introduction

The Athabasca Oil Sands Region (AOSR) in northeastern Alberta, Canada contains proven economically recoverable bitumen reserves estimated to be 165 billion barrels in 2016 (Alberta Energy Regulator, 2017). Oil production in the AOSR has increased from 0.6 million barrels per day in 2000, to 2.5 million barrels per day in 2016 (Alberta Energy, 2017) despite significant production interruptions due to the Horse River Wildfire in May of that year (Landis et al., 2018). Synthetic crude oil production from bitumen in the AOSR is accomplished using a combination of surface mining and in situ (drilling) production. Surface mining in the AOSR results in large-scale land disturbance similar to conventional open pit mining operations. The soil overburden overlaying the oil sand deposits is removed and the exposed oil sands are excavated and transported using large-scale shovel and truck hauling operations. Atmospheric pollution from shovel and truck fleet operations mainly consists of fugitive particulate matter (PM) emissions (wind-blown dust) and diesel engine combustion exhaust (Landis et al., 2012; Wang et al., 2015; Wang et al., 2016). Bitumen is separated from the sand and clay matrix components of the oil sands using a warm water separation technique (Masliyah et al., 2004; Osacky et al., 2013), and in four of the current commercial operations is upgraded to sweet light synthetic crude on site. Upgrading by-products, such as elemental sulfur and petroleum coke, are in many cases consolidated in large onsite storage piles that have been identified as significant sources of fugitive dust in the AOSR (Zhang et al., 2016).

The emission of polycyclic aromatic hydrocarbons (PAHs) and polycyclic aromatic compounds (PACs) from oil production activities and subsequent atmospheric deposition has been a focal point for researchers in the AOSR due to their potential for human and ecological toxicity (Harner et al., 2018). PAH concentrations in ambient air, snow, surface waters, sediments, and wildlife have suggested that surface mining and in situ bitumen production, as well as onsite upgrading activities are contributing to the environmental burden in the AOSR (Kelly et al., 2009; Kurek et al., 2013; Bari et al., 2014; Schindler, 2014; Ahad et al., 2015; Schuster et al., 2015; Lundin et al., 2015; Birks et al., 2017; Boutin and Carpenter, 2017). Recent studies have begun to focus on the origins of PAHs and PACs in environmental samples and strategies for the mitigation of environmental impacts in the AOSR (Ahad et al., 2015; Jautzy et al., 2015; Korosi et al., 2016; Zhang et al., 2016; Manzano et al., 2017). PACs in particular are well-established markers for differentiating petrogenic, pyrogenic, and biogenic sources (Wang et al., 1999, 2009: Wang and Fingas, 2003) and have been shown to be useful for source characterization and differentiation in the AOSR (Yang et al., 2011, 2014).

The AOSR is located in a remote boreal forest ecosystem. Much of the region surrounding the bitumen production facilities has limited or no access by surface roads and lacks commercial electric power infrastructure. Active ambient monitoring is limited to a relatively narrow north/south transportation corridor through the center of active oil sands production operations in the region. Therefore, the epiphytic lichen, *Hypogymnia physodes,* predominantly growing on jack pine (*Pinus banksiana*) and black spruce (*Picea mariana*), is being used as a bioindicator of the atmospheric deposition and integrative accumulation of air pollutants for a Wood Buffalo Environmental Association (WBEA) Terrestrial Environmental Effects Monitoring (TEEM) program at a broader spatial scale (Foster et al., 2019). The *H. physodes* was selected because it is a well-established bioindicator for characterizing atmospheric deposition, collects all its nutrients from the air, has a high tolerance for air pollution (e.g., SO_2), is prevalent in all areas of the AOSR, and was determined to be the optimum species for air quality monitoring of PAHs and trace elements in the AOSR (Garty, 2001; Jeran et al., 2002; Graney et al., 2017).

A lichen biomonitoring and source apportionment study conducted in 2008, that was focused primarily on inorganic air pollutants, concluded that fugitive dust emissions from oil sand production activities (e.g., haul road emissions, raw oil sand and processed materials, tailing sand) were the primary sources of the observed atmospheric deposition and observed spatial gradients of total sulfur, major elements, and many trace elements in the AOSR (Edgerton et al., 2012; Graney et al., 2012; Landis et al., 2012). An initial pilot study focused on PAH deposition involving the selection of a subset of twenty of the 2008 *H. physodes* samples found (i) the sum of measured PAH congener concentrations (ΣPAH) ranged from 52 to 352 ng g^{-1}; (ii) phenanthrene and naphthalene were the predominant compounds present with median concentrations of 22.1 and 18.0 ng g^{-1}, respectively; (iii) ΣPAH were highly correlated with crustal and petrogenic elements associated with anthropogenic fugitive dust sources; and (iv) the highest PAH concentrations were observed in close proximity (<40 km) to the major oil sands mining and upgrading operations (Studabaker et al., 2012).

This paper presents results from a comprehensive 2014 *H. physodes* bioindicator source apportionment follow-up study designed to investigate the sources and spatial distribution of PAH atmospheric deposition in the AOSR.

2. Methods

2.1. Study design

Lichen samples were collected within an approximate 150 km radius from the center of AOSR oil sand production operations using a scaled (nested) approach in a similar conceptual framework as a previous large scale AOSR lichen collection study in 2008 (Edgerton et al., 2012). The goal was to collect samples from a higher density of sites closest to the major surface mining and processing operations where steep deposition gradients have previously been observed with a decreasing density as the distance from the oil sands production areas increased. Appendix Table A.1 summarizes the *H. physodes* sample locations categorized as a function of their minimum distance from either a surface oil sand mining or processing site. Due to the distances, rough terrain, and lack of surface roads, helicopter access was the method of transportation to and from remote sampling sites. The lichen sampling collection strategy was to (i) resample as many sites as possible from the 2008 lichen study while complying with the new AOSR helicopter safety landing regulations and (ii) sample from new sites to ensure adequate spatial coverage within the 150 km radius sampling domain.

Lichen samples from 127 sites were collected from (i) jack pine dominant (n = 80) and (ii) black spruce dominant (n = 47) stands (Fig. 1; Appendix Table A.2). Previous WBEA AOSR lichen bioindicator studies in 2002, 2008, and 2011 preferentially utilized dry (jack pine) ecosite stands; and the continuation of this collection strategy will allow for future temporal trend comparisons at these common sites. However, wet (black spruce) ecosite stands were also sampled to meet the spatial distribution sampling goals of this study. The 2008 *H. physodes* receptor modeling study focused on inorganic pollutants (Landis et al., 2012) and found no significant difference between lichens collected from black spruce and jack pine stands for the major AOSR sources. As a result, the lichen sampling collection strategy for this study was a combination of (i) resampling sites from previous lichen studies (Berryman et al., 2004; Berryman et al., 2010; Edgerton et al., 2012) where possible, (ii) WBEA Terrestrial Environmental Effects Monitoring (TEEM) forest health and passive air quality monitoring sites (Foster et al., 2019), and (iii) sites of opportunity that filled in the spatial domain and presented safe helicopter landing locations.

2.2. Oil Sands production source locations

Due to the historical oil sands production activities being located in a central area, a sampling location identified as AR6 located between the Suncor and Syncrude upgrader stacks (Appendix Fig. B.1) has been previously used to investigate spatial atmospheric deposition patterns in the AOSR (Kelly et al., 2009; Kelly et al., 2010; Graney et al., 2012; Landis et al., 2012; Kurek et al., 2013; Kirk et al., 2014). New oil sand production and support operations have since come online in the AOSR. To address this, all significant emission sources and their impact on the spatial distribution patterns of atmospheric deposition were located and identified for this study. This included nineteen relevant major emission sources related to surface mining and upgrading of oil sands in the AOSR (Appendix Table A.3; Appendix Fig. B.1). Source locations were initially drawn from environmental impact assessment (EIA) documents and verified/updated as necessary to reflect operational conditions in 2014 using Google Earth Professional version 7.3.1 and commercially available satellite imagery from the time period (April 2–August 11, 2014; Digital Globe & CNES/Airbus). Most large area

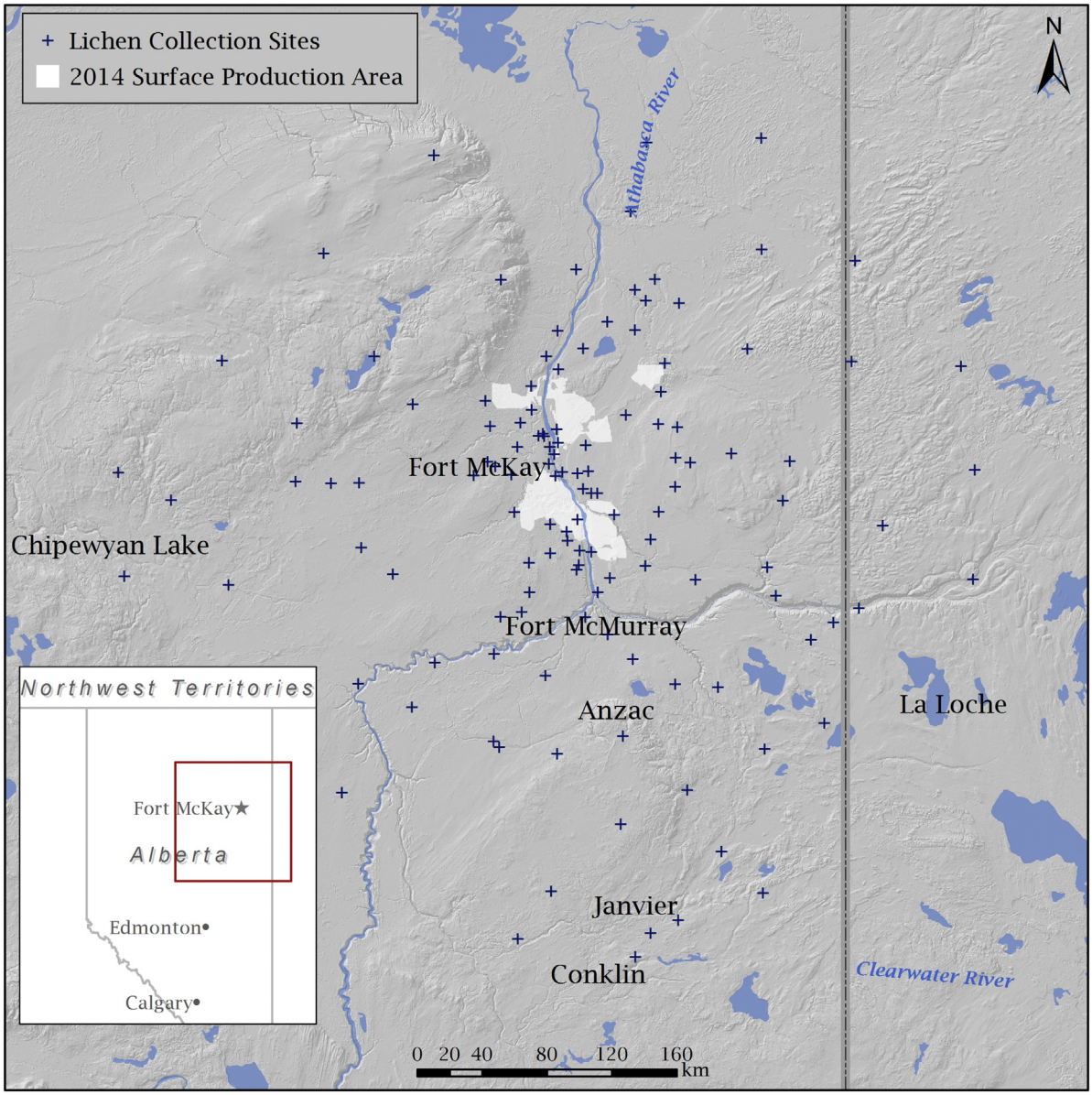

Fig. 1. Map Depicting the Location of the 2014 Lichen Collection Sites and the Areal Footprint of Major Surface Oil Sand Bitumen Production Facilities Operating during the Study Period.

sources (e.g., mines, quarries, storage piles) were located at their activity center point rather than an area perimeter for simplicity. However, in some cases multiple oil sand mine locations within a single producer operation were included in the spatial analysis due the size and areal extent of their operations.

2.3. Collection of lichen samples

Bulk composite samples of *H. physodes* were collected from the branches of a minimum of 10 standing jack pine or black spruce trees at approximately 1.5 m off the ground at each sampling site. Field personnel wearing vinyl gloves carefully extracted the lichens from each tree such that the sample was representative of the overall community structure (e.g., specimen size distribution) using Teflon-coated forceps until several grams of lichen mass were collected. Lichens collected from all of the trees were composited into the same, pre-cleaned 500 ml amber glass jar (Fisher Scientific; #02-993-053), labeled with a tracking number representing the site and date of collection, then stored in a cooler for the duration of the day. Replicate *H. physodes* samples were collected at 13 sites to characterize within-site variability of the sample collection and analysis methodology.

In the WBEA Field Operations Center, lichen thallus samples were cleaned by removing foreign materials (bark and other debris) under a clean hood and transferred into a clean 250 ml amber glass jar (Fisher Scientific; #05-721-102). The goal was for the cleaned sample to yield ~5 g of mass required for all analyses, lab replicates, and archival. Cleaned samples were shipped to RTI International (Research Triangle Park, NC) where an aliquot of each sample for extraction and PAH analysis was removed. The balance of each sample was then shipped to the University of Michigan (UM; Ann Arbor, MI, USA) for grinding in a zirconium ball mill to prevent contamination of the samples with trace elements of interest that are typically present in stainless steel (e.g., Fe, Cr, V, Ni). After grinding, UM forwarded samples to Atmospheric Research & Analysis (ARA; Morrisville, NC) for elemental analysis, and to Pacific Soils Analysis Inc. (PSAI; Vancouver, British Columbia) for total sulfur and total nitrogen analysis.

H. physodes samples were stored (i) frozen (−30 °C) between every step in the collection, cleaning, grinding, extraction, and analysis, and (ii) no active drying of the samples was conducted to minimize the loss of semi-volatile PAH/PAC compounds. We assessed the impact of moisture content on a subset of 21 sample sites comparing "as collected" to oven dried mass. Triplicate samples from each site of approximately 100 mg were weighed on a 5-digit scale (Mettler-Toledo Model MS205PU) and then heated in a laboratory oven at 75 °C for 24 h. Samples were re-weighed after cooling to room temperature. Results (see Appendix Table A.4) show that the mean mass loss on oven dried *H. physodes* samples was $-3.3 \pm 1.3\%$ with a range of 0.8–5.6%. These mass losses are negligible compared to the range of concentrations observed across lichen samples (hundreds of percent), and, therefore, do not appreciably affect reported mass concentrations and source apportionment results.

2.4. Lichen sample extraction and organic analysis

The method used for the extraction, cleanup, and determination of PAHs and PACs in lichen thallus by gas chromatography with time-of-flight mass spectrometry (GC-TOF-MS) has been described previously (Studabaker et al., 2017). In short, approximately 0.5 g lichen sample was milled in liquid nitrogen to yield a fine powder. Milled *H. physodes* (0.2 g) was weighed into a scintillation vial, spiked with deuterium-labeled internal standards, and extracted three times with cyclohexane in an ultrasonic bath. The combined extracts were concentrated, cleaned on 1 g silica gel, adjusted to a final volume of 0.2 ml, and transferred to an autosampler vial. Quantitative analysis was performed on a LECO (Saint Joseph, MI) Model Pegasus 4D GC-TOF-MS equipped with a DB5-MS column (60 m × 0.25 mm × 0.25 μm). PAHs, 1- and 2-methylnaphthalene, dibenzothiophene, and retene were calibrated using minimum 7-point standard curves. Benzo(*b*)fluoranthene and benzo(*j*)fluoranthene were incompletely resolved and are reported together as benzo(*bj*)fluoranthene. Chromatographic peaks for 1- and 4-methyl dibenzothiophene and the chromatographically unresolved pair 2- and 3-methyldibenzothiophene were assigned using mass spectral profiles and literature values for their retention indices and quantitated using 2-dibenzothiophene as a reference. Other PACs were integrated as one or more groups, identified using mass spectral profiles, and quantitated based on the calibration of representative reference compounds (e.g., C1-phenanthrenes were quantitated based on the calibration of 2-methylphenanthrene).

In this paper PACs refer to C1- and C2-alkyl PAHs, dibenzothiophene, and the C1- and C2-dibenzothiophenes. Alkyl PAHs are normally assigned to groups and named based on the level of alkylation of the parent PAH or one member of a group of structural isomers. Thus, methylphenanthrenes and methylanthracenes are included in the C1-phenanthrenes, dimethylnaphthalenes and ethylnaphthalenes are included in the C2-naphthalenes, up to C4-PAHs for some groups (Wang and Fingas, 2003). For analytical reasons (Studabaker et al., 2017), we limited our investigation to dibenzothiophene and C1- and C2-PACs. Retene (a C4-phenanthrene) was the only exception; it was included for source apportionment purposes since it is a widely used tracer analyte for coniferous biomass combustion (Ramdahl, 1983; Schauer et al., 1996; Simoneit, 2002) and wildfires are a large natural source of PM and PAHs in the AOSR (Bytnerowicz et al., 2016; Landis et al., 2017; Landis et al., 2018; Wentworth et al., 2018). Retene is unique among many of the other C4 Alkyl PAHs in that it elutes early as an easily distinguishable peak and does not have any observed interferences in our *H. physodes* sample matrix. We treated retene separately from the other PACs and it is not included in subsequent ΣPAC calculations.

In this work we refer to the sum of the 16 EPA priority PAH concentrations and benzo(*e*)pyrene as ΣPAH, while the sum of the 17 PAC concentrations is referred to as ΣPAC. The sum of both ΣPAH and ΣPAC is referred to as ΣPAH + PAC.

2.5. Lichen sample extraction and elemental analysis

The extraction and analysis of *H. physodes* samples for elemental composition has been previously described by Edgerton et al. (2012). Briefly, homogenized aliquots (25–35 mg) were digested in a sequential peroxide and acid addition procedure similar to that developed by Jalkanen and Häsänen (1996) using a MARS Express (CEM Corp., Matthews, NC) microwave digestion system. The first digestion step included the addition of 2.0 ml of 30% ultrapure H_2O_2 (J.T. Baker Ultrex-II) with heating to 100 °C for 10 min to break down organic matrices. After cooling, 1.0 ml of ultrapure HNO_3 (J.T. Baker Ultrex-II) and 0.25 ml of ultrapure HF (J.T. Baker Ultrex-II) was added to each vessel and heated to 180 °C for 10 min to dissolve the mineral matrices. After cooling, 5 ml of ASTM Type I ultrapure (18.2 MΩ · cm) water was added to each vessel and heated to 180 °C for 20 min. Digestates were then vacuum filtered through a Whatman #541 ashless paper filter and brought up to a final volume of 25 ml with ultrapure water. Two to three digestion blanks, two to three replicate samples, and one to two aliquots each of two standard reference materials (SRMs) were included in each batch. The SRMs utilized were: (i) Community Bureau of Reference (BCR) 482 (elements in lichens), and (ii) National Institute of Standards and Technology (NIST) 1633c (coal fly ash). The sample size of digestion aliquots for BCR 482 and NIST 1633c were 25–30 mg.

The determination of the elemental content in lichen thallus samples was performed using a Perkin-Elmer (Waltham, MA) Model Elan-II dynamic reaction cell inductively coupled plasma mass spectrometer (DRC-ICPMS). Clean handling techniques were used in all stages of the analysis to prevent contamination. Particle-free gloves were worn at all times and all labware with which the samples and reagents come

into contact was acid cleaned. Just prior to analysis, a portion of each sample aliquot was transferred to a 10 ml polypropylene auto sampler vial. The samples were introduced by pneumatic nebulization. Peak characteristics for each target element were considered in the method to eliminate interferences from polyatomic ions derived from the plasma gas, reagents, or sample matrix. Instrument drift and suppression, or enhancement of instrument response caused by the sample matrix, were corrected by internal standardization.

Elemental recoveries for 22 elements in reference samples (NIST 1633c and BCR 482) are listed in Appendix Table A.5. Recoveries are within 20% of certified values for all elements and within 10% of certified values for all elements except Cd, Cr, Pb (BCR 482 only) and Ti. Standard deviations are generally <10%, indicating good reproducibility of recoveries, even for relatively small aliquots of each SRM (e.g., ~25 mg). As shown previously (Edgerton et al., 2012), results of SRM digestions show that the H_2O_2/HF/HNO_3 microwave digestion protocol effects near-quantitative recovery of elements from both the mineral matrix (NIST 1633c) and the plant matrix (BCR 482).

2.6. Lichen total sulfur and total nitrogen analysis

Total-S concentrations in cleaned and ground *H. physodes* thallus samples were determined by PSAI with a LECO Model S144-DR Sulfur Determinator using dry combustion and infrared detection of a 100–150 mg lichen sample aliquot covered by tungsten oxide in an oxygen atmosphere at 1350 °C. The sulfur detector was calibrated with three LECO plant reference materials (LECO 1026, orchard leaves; LECO 1025, orchard leaves; LECO 1010, tobacco leaves). Total-N concentrations were determined with a LECO Model FP-528 Nitrogen Analyzer by dry combustion and thermal conductivity of a 150–500 mg aliquot of lichen in a gel capsule. The nitrogen analyzer was calibrated using three LECO plant reference materials (LECO 1006, rice flour; LECO 1026, orchard leaves; and, LECO 1052, ethylenediaminetetraacetic acid).

2.7. Source apportionment modeling

Source apportionment is the estimation of contributions to the pollutant concentrations resulting from emissions from multiple natural and anthropogenic sources (Hopke, 2009; Hopke, 2016). Statistical source apportionment analysis tools (e.g., receptor models) are applied to extract information on the sources of air pollutants from the measured constituent concentrations at a receptor location, which in this study are the lichen samples. Unlike deterministic dispersion air quality models, receptor models generally do not use pollutant emissions, meteorological data, or chemical transformation mechanisms to estimate the contribution of sources to receptor concentrations. Instead, receptor models use mathematically detectable characteristics (chemical and physical) at a monitoring or receptor site to both identify and quantify source contributions to receptor concentrations. The multivariate EPA Positive Matrix Factorization (PMF) v5.1 receptor model (U.S. Environmental Protection Agency, 2014a) was used for this study. Briefly, the EPA implementation of PMF uses a graphical user interface that has been developed on the PMF model, and the general mixed linear model is solved using the Multilinear Engine-2 (ME-2) program (Paatero, 1999). EPA PMF operates in a robust mode, meaning outlier analyte concentrations are not allowed to overly influence the factor solutions. Additionally, the feature of individual weighting of each data point allows the model to calculate covariance in the receptor data matrix on the basis of reliability of the chemical measurements.

Since the *H. physodes* data were not accompanied by point-wise concentration analytical uncertainties, measurement errors were estimated from the respective GC-TOF-MS, LECO, and DRC-ICPMS MDL and laboratory duplicate analysis precision data (U.S. Environmental Protection Agency, 2014b). Below MDL analyte concentrations were replaced by 1/2 of the MDL, and its uncertainty was estimated as (5/6) × MDL (Polissar et al., 1998). If the measured concentration was >MDL, then uncertainty was estimated using Eq. (1) (Polissar et al., 1998).

$$Uncertainty = \sqrt{\left(\frac{5}{6} \times MDL\right)^2 + (Conc \times RPD)^2} \quad (1)$$

where RPD = mean relative percent difference of n (7–11) laboratory duplicate sample analysis.

Chemical analytes with a signal-to-noise ratio < 1 (as calculated by EPA PMF5.1) were excluded from modeling. Acenaphthene, dibenz(*a*,*h*)anthracene, benzo(*c*)phenanthrene, benzo(*k*)fluoranthene, C1-fluoranthenes/pyrenes, benzo(*a*)pyrene, dibenzo(*a*,*h*)pyrene, dibenzo(*a*,*l*)pyrene, Pt, and Pd were in this category. Because of higher abundances and superior analytical performance, signal-to-noise ratio for crustal elements (Ba, Sm, Ce, As, Sr, Fe, Mn) and oil markers (V, Mo) were ≥ 9. To avoid inorganic data overly influencing the factor solutions, all of these elements were set as 'weak'. Cs, Mg, Na, Co, Pr, and Nd were excluded from modeling as source types represented by these analytes were adequately represented by the presence of other included crustal (Al, Si, Ti) and oil sand (Ce, La, Sm) elements. Be, Sn, Bi, W, Th, Tl, and U were excluded due to their low concentrations (Appendix Table A.6) and their known analytical challenges. The final PMF model was run using a total of 52 analytes (13 PAHs, 13 PACs, 25 elements, and retene) from the 127 *H. physodes* samples.

Two error estimation methods for analyzing factor analytic solutions were used to evaluate the PMF model runs: (i) bootstrap analysis (BSA) which captures random errors; and (ii) displacement analysis (DISP) which deals with errors associated with factor rotational ambiguity (USEPA, 2014a). Using objective numerical tools eliminates the subjective selection of factor numbers (EPA, 2014a) and minimizes factors that do not correspond to real source types (Henry et al., 1984; Park et al., 2000).

The PMF model generated factors and their linkages to real world sources are identified based on what was known about the physical and chemical characteristics of known emission sources. In many cases these identifications are based on published source profiles (e.g., Clearinghouse for Inventories and Emission Factors - Speciate Version 4.4 (EPA, 2014b)). In this study, contemporary source profiles generated locally in the AOSR (Landis et al., 2012; Wang et al., 2015; Wang et al., 2016; Jariyasopit et al., 2018; Harner et al., 2018) were also utilized to reduce the likelihood of misidentification of source types. In addition, a modified pyrogenic index (PI; Wang et al., 1999; Wang and Fingas, 2003) from PAH and PAC analyte concentrations in each factor profile was calculated as: sum of select PAH and PAC congeners (naphthalene + fluorene + dibenzothiophene + phenanthrene + chrysene + the C1- and C2-PACs for each of parent PAHs)/sum of other PAHs (anthracene + fluoranthene + pyrene + benz(*a*)anthracene + benzo(*bj*)fluoranthene + benzo(*e*)pyrene + indeno (1,2,3-*c*,*d*)pyrene + benzo(*g*,*h*,*i*)perylene). The modified PI value was used to categorize factors as either petrogenic (petroleum derived; PI < 0.1) or non-petrogenic (combustion derived; PI > 0.2). The non-petrogenic designation includes petroleum coke sources. Petroleum coke is a residue from the upgrading of heavy bitumen to light synthetic crude oil. The thermal cracking process is conducted in the absence of oxygen making it distinct from fossil fuel combustion, so that petroleum coke exhibits a distinct organic profile compared to soot. Calculation of both the Wang PI and the modified PI for source materials showed that raw AOSR oil sands yield a PI <0.10, while petroleum coke yields values >0.2; values for purely pyrogenic sources may be >1 (Wang et al., 1999).

2.8. Spatial interpolation and plotting

Lichen concentrations and source apportionment model (PMF) source contribution estimates (SCEs) were spatially interpolated onto

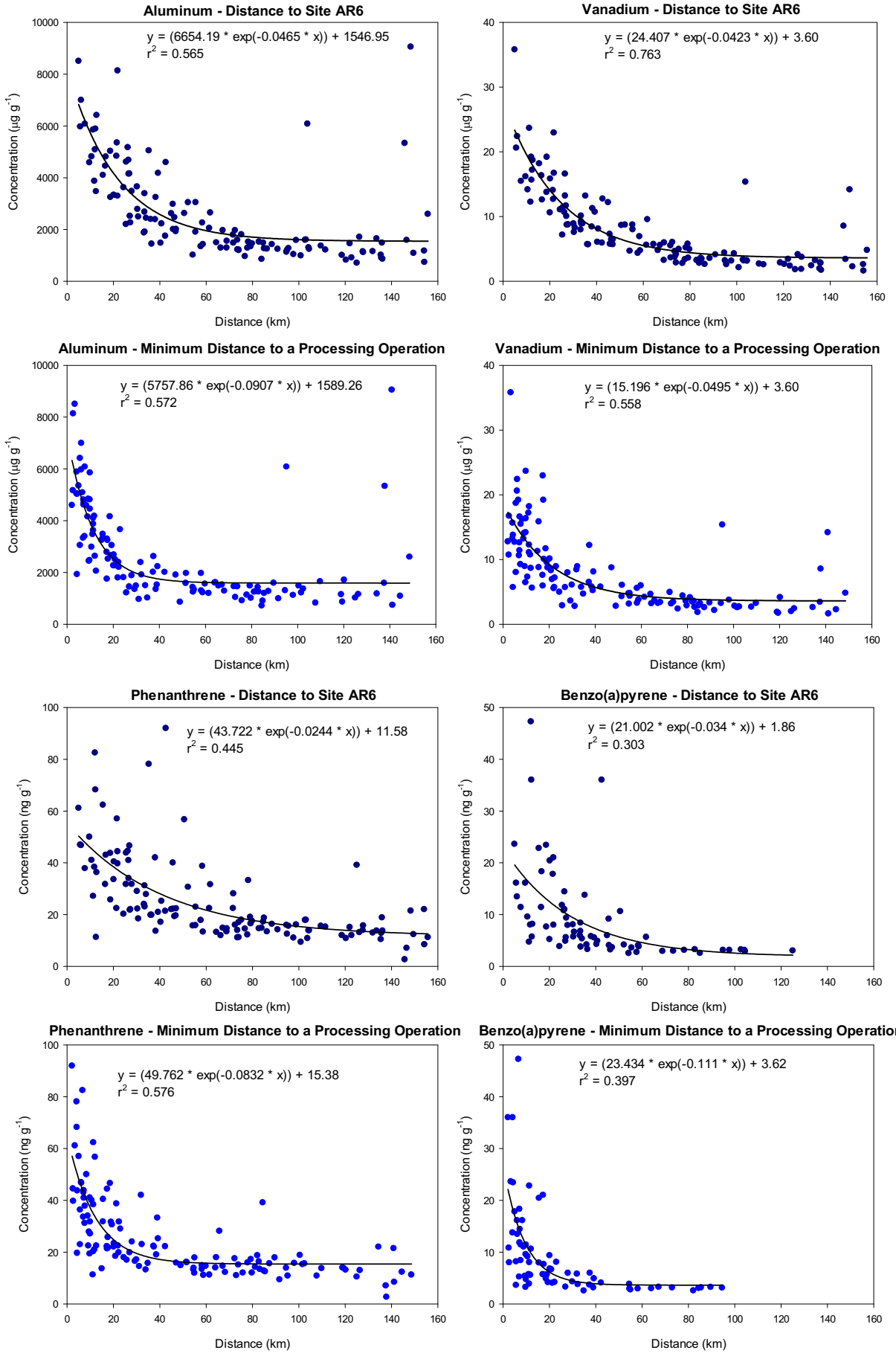

Fig. 2. Differences in *H. physodes* Concentrations vs Distance from a Site Between the Two Main Upgrading Stacks (AR6), and the Nearest Surface Oil Sands Production Site.

the AOSR sampling domain using Surfer (Golden Software, Golden, CO) version 15 and overlaid onto an ArcGIS (ESRI, Redlands, CA) version 10.5 base-map specifically created for this study. The ArcGIS base map used for the spatial interpolation plots includes locations of major roadways and rivers, lichen sampling locations, as well as Fort McKay, Fort McMurray, and other communities to assist in interpretation of concentration gradients. Google (Mountain View, CA) Earth Professional version 7.3.1 was used to locate lichen sample collection site locations and visually evaluate local sources of resuspended dust using time relevant surface satellite images.

3. Results and discussion

3.1. Lichen PAHs and PACs analytical results

As in the 2008 (Studabaker et al., 2012) and 2014 (Graney et al., 2017) pilot studies, the highest concentrations of PAHs were found in close proximity to surface oil sand production facilities, with concentrations rapidly declining and approaching near constant values at distances >25–50 km from major oil sand production operations (Fig. 2). A summary of PAH concentrations above MDL are presented in Table 1 for *H. physodes* samples collected from the 127 locations in the AOSR study domain. Of the 21 PAH compounds analyzed, naphthalene, fluorene, phenanthrene, fluoranthene, pyrene, benzo(*a*)anthracene, chrysene, benzo(*bj*)fluoranthene, and benzo(*g*,*h*,*i*)perylene concentrations were above the MDLs in >90% of the lichen samples. This was a significant achievement from an analytical perspective for the small amount of sample (200 mg) used for analysis and the low concentrations of PAHs in most of the samples observed in this study.

Our study design expanded on previous pilot studies of PAH deposition in the AOSR, which showed a rapid decline in PAH concentrations in lichens with increasing distance from the surface oil sands operations, with decreases in total PAHs of up to an order of magnitude measured at locations >50 km from the nearest operations (Studabaker et al., 2012; Graney et al., 2017). This deposition pattern has been observed for other markers of emissions in the AOSR (Edgerton et al., 2012; Graney et al., 2012; Landis et al., 2012; Graney et al., 2017), and has been ascribed primarily to fugitive dust emissions associated with mining, hauling, upgrading, and stock piling operations (Landis et al., 2012; Ahad et al., 2014; Zhang et al., 2016). Effective interventions to reduce regional impacts of emissions depend on identifying the most important sources of those emissions. Thus, the gradient is important in two respects: the abundance of quantifiable PAH markers close to the surface oil sand production operations permits differentiation of multiple sources within the operations area, and the size of the "footprint" within the total study area is small enough to permit identification of regional sources outside the operations area, that would not be influenced by operations-associated interventions.

The PAH data may be interpreted in the context of earlier 2008 (Studabaker et al., 2012) and 2014 (Graney et al., 2017) pilot studies, as well as other studies employing epiphytic lichens as PAH accumulators. Of particular importance is evaluating the *H. physodes* PAH concentrations as coincident measures of PAH atmospheric deposition, within and across studies. The simplest metric to use in making comparisons between or across studies is the sum of the concentrations of all measured PAHs (ΣPAH). Such comparisons can be inexact due to (i) the variable number of analytes that may be included in ΣPAH, (ii) inclusion of more analytes than the 16 USEPA PAHs, (iii) inclusion of fewer analytes (possibly due to non-detects), (iv) differing approaches to accounting for non-detects and values below the quantitation limit (which may vary significantly across studies), and (v) proximity, intensity, and seasonality of sources. Typically, however, similar PAH compounds (e.g., phenanthrene, fluoranthene, chrysene) predominate in samples across studies, and are reported in the calculation of ΣPAH.

ΣPAH in *H. physodes* collected during the current study ranged from <20 ng g^{-1} to >400 ng g^{-1}. That range is consistent with ranges from the 2008 and 2014 pilot studies and is generally lower compared to PAH concentrations that have been reported in studies of lichen PAH bioaccumulation in Europe (Appendix Table A.7). Care was taken when making this comparison as many experimental variables that differ across studies may impact the measurements made even when comparable rigor is applied across sampling techniques, sample cleaning, and quality assurance procedures (Van der Wat and Forbes, 2015). Factors such as differences across chemical analytes in absolute and relative adsorption and retention of vapor phase and PM-associated PAHs, seasonal variation in uptake and retention of PAHs relative to the lichen species collected, times of sample collection, and methodological differences that may impact completeness of extraction or introduction of matrix components that interfere with analyte measurement, can contribute to significant differences in measurements. The impact of target lichen species selection on measurement of ΣPAH is illustrated by the data from the 2014 pilot study (Graney et al., 2017), where PAH measurements of five different epiphytic and ground lichen species collected at the same site varied by more than a factor of 4 (Appendix Table A.7).

Of the 17 individual PAC analytes and groups included in this study, all but C1-benzopyrenes and C2-chrysenes were found at concentrations above the MDL in >90% of the samples. The 2-methylnaphthalenes, C2-naphthalenes, C1– and C2-phenanthrenes, and retene were found in every sample. Mean measured concentrations across analytes and analyte groups ranged from 5.7–69 ng g^{-1}, with maximum concentrations for C2-phenanthrenes and C2-chrysenes >300 ng g^{-1}. As was the case for PAHs, concentrations of PACs declined with increasing distance from oil sands operations. These data constitute the first use of epiphytic lichens as PAC bioaccumulators.

3.2. Lichen inorganic analytical results

The DRC-ICPMS and LECO derived inorganic MDLs and ratios of minimum and median observed concentrations to MDLs for 45 elements in *H. physodes* are summarized in Table Appendix A.6. MDLs for the major elements (e.g., total sulfur, total nitrogen, Al, Si and Fe) are in the range 1–200 μg g^{-1}, while those for the rare earth elements and platinum group elements are generally <0.01 μg g^{-1}. Minimum observed concentrations across all samples were greater than MDL for all elements, except Be, Pd, Pt, Ta and Bi (Appendix Table A.6). Median concentrations were at least 10 times MDL for all elements, except Be, Sb, Pt, Ta and Sn. These results indicate that we have a robust set of inorganic analytes for determination of spatial patterns and source attribution.

Precision data for 45 elements in *H. physodes* are presented in Appendix Table A.8. Instrument RSD is the mean relative standard deviation of within-sample replicate measurements (n = 127). Laboratory absolute percent difference (APD) is the mean absolute percent difference of duplicate analyses of individual lichen samples (n = 7). These data provide a measure of sample heterogeneity. Field APD is the mean absolute percent difference of separate samples collected from the same field site (n = 13). These data illustrate the combined effects of sample heterogeneity and site heterogeneity. Not surprisingly, results show that Instrument RSD < Lab APD < Field APD. Lab APDs indicate that most elements are measured in individual samples with an overall precision of 5–10%. Field APDs indicate that individual sites were characterized with overall precision of <10–20%. Exceptions to this include low concentration elements previously mentioned (e.g., Be) and Cu. Inspection of data for Cu show that it was well behaved in terms of instrument RSD and sample APD and was well above MDL in all samples, but that field replicates from two sites (150B9 and AMS15) had high APDs. If these two sites are treated as outliers, then the Field APD for copper decrease from 20% to 6%. In general, data in Appendix Table A.8 support the conclusion that fairly modest (e.g., ±50%) differences in element concentrations should be easily detectable, and statistically significant, using the above analytical techniques.

Table 1
Statistical Summary of PAHs in Lichens Above the MDL (ng g^{-1}).

Analyte	MDL	n	Mean	Std Dev	Min	Q1	Median	Q3	Max
Naphthalene	3.4	125	8.23	3.36	3.82	5.68	7.28	9.87	23.30
Acenaphthylene	0.30	30	0.42	0.12	0.31	0.34	0.37	0.44	0.70
Acenaphthene	0.29	93	1.20	2.58	0.32	0.56	0.80	1.22	25.30
Fluorene	0.31	127	3.16	1.33	1.11	2.34	2.89	3.65	10.00
Phenanthrene	0.28	127	25.19	15.98	2.61	13.95	19.60	31.75	91.90
Anthracene	0.52	93	2.66	2.73	0.55	0.98	1.57	3.26	15.8
Fluoranthene	0.69	127	7.74	3.47	1.18	5.41	6.88	9.14	22.70
Pyrene	0.12	127	6.53	6.89	0.44	2.38	3.66	8.28	37.70
Benzo(*c*)phenanthrene	0.34	42	1.22	0.85	0.35	0.69	0.91	1.47	4.19
Benz(*a*)anthracene	0.26	122	5.45	7.06	0.32	1.34	2.89	6.01	42.40
Chrysene	0.44	126	10.91	13.82	0.61	2.98	5.90	12.10	83.20
Benzo(*bj*)fluoranthene[a]	0.66	119	7.65	4.90	1.55	3.90	6.47	9.88	29.90
Benzo(*k*)fluoranthene	2.5	7	3.11	0.73	2.50	2.75	2.77	3.26	4.66
Benzo(*e*)pyrene	0.55	102	6.65	7.31	0.82	2.47	3.65	8.45	41.90
Benzo(*a*)pyrene	2.5	71	9.30	8.57	2.52	3.76	5.78	11.40	47.25
Indeno(1,2,3-*c*,*d*)pyrene	2.5	17	5.13	2.18	2.59	3.66	4.81	5.26	11.10
Dibenz(*a*,*h*)anthracene	2.5	26	5.97	3.92	2.68	3.29	5.10	6.84	18.20
Benzo(*g*,*h*,*i*)perylene	2.5	46	7.46	5.60	2.66	4.12	5.54	8.56	28.30
Dibenzo(*ai*)pyrene	2.5	15	4.10	1.52	2.67	3.16	3.63	4.36	8.58
Dibenzo(*al*)pyrene	2.5	1	2.77	.	2.77	2.77	2.77	2.77	2.77
Dibenzo(*ah*)pyrene	2.5	1	2.74	.	2.74	2.74	2.74	2.74	2.74
1-Methylnaphthalene	0.81	127	11.06	5.17	1.66	8.10	10.19	12.30	40.05
2-Methylnaphthalene	0.51	127	5.35	2.13	0.81	4.11	4.93	5.98	16.50
C1-Fluorenes	0.57	126	7.76	5.37	0.58	4.25	5.88	10.07	33.00
Dibenzothiophene	0.17	126	5.70	6.62	0.45	1.58	3.19	7.32	44.60
4-Methyldibenzothiophene	0.23	125	13.60	15.04	0.89	3.32	7.55	18.50	90.55
Dibenzothiophene, 2/3-methyl-[a]	0.23	123	9.14	10.73	0.47	2.02	4.92	11.70	63.80
1-methyldibenzothiophene	0.23	119	7.17	7.80	0.32	1.45	4.4	11.4	38.75
C1-Phenanthrenes	0.98	127	50.58	44.72	3.04	21.25	29.95	66.20	238.00
Retene	1.02	127	21.84	10.29	1.43	14.25	20.10	28.10	50.80
C1-Fluoranthenes/pyrenes	0.59	125	19.95	18.58	3.77	9.02	13.20	22.35	113.00
C1-Chrysenes/isomers	0.59	123	32.82	41.16	1.47	7.98	16.70	39.05	244.50
7-Methylbenzo(a)pyrene/C1-BPs/BFs	2.5	56	57.64	44.85	10.30	21.55	44.23	82.60	196.50
C2-Naphthalenes	0.45	127	26.77	12.46	3.80	20.00	25.40	32.10	76.90
C2-Dibenzothiophenes	2.5	124	45.28	49.85	2.93	9.89	21.28	65.50	263.50
C2-Phenanthrenes/anthracenes	2.5	127	69.32	60.35	7.18	28.05	41.90	94.70	303.00
C2-Fluoranthenes/pyrenes	2.5	117	40.50	42.58	3.11	14.60	25.60	54.55	234.50
C2-Chrysenes/isomers A	2.5	107	51.13	55.20	3.52	16.40	30.70	62.70	302.50

[a] Sum of two co-eluding isomers.

A summary of elemental concentrations above MDL is presented in Table 2. Of the 45 elements analyzed, 40 were above MDL in all of the lichen samples. The exceptions were low concentration elements including Be, Pd, Pt, Ta, and Bi (Appendix Fig. B.2). The number of elements quantified and the number of sites included in this study comprise a significant contribution to the understanding of regional dispersion, deposition, and accumulation of elements from an industrial complex. The maximum versus 25th percentile (Q1) concentration was >10 for W, Sn, Sb, Mo, Li, Bi, Th, Ca, Ta, La, V, Nb, Ce, and Pr (Appendix Fig. B.3). This suggests that the maximum versus quartile 1 (25th percentile) element concentration ratios reflects near source enhancement in elemental concentrations, and the ratio can be used as a means to express the scale of the enhancement in near source concentrations related to distal site concentrations. Tl, Cd, Ba, Mg, total sulfur, Pb total nitrogen, Rb, Zn, P, and K had maximum/quartile 1 concentration ratios less than five. These low enhancement factors represent other factors that influence element incorporation and sequestration within *H. physodes*. These factors will be explored in more detail in subsequent discussion sections.

3.3. Spatial results

A number of studies have reported elevated atmospheric deposition flux of inorganic and organic analytes as a function of distance to the center of surface oil sands production operations (Kelly et al., 2009; Graney et al., 2012; Landis et al., 2012; Studabaker et al., 2012; Kurek et al., 2013; Kirk et al., 2014; Graney et al., 2017). A common way to assess proximal enhancement versus distal regional baseline in atmospheric deposition flux in the AOSR is through use of deposition/concentration versus distance trend plots. The inorganic element plots in Fig. 2 depict the relationship between *H. physodes* concentration (μg g^{-1}; y-axis) and distance (km; x-axis) from a point between the two main upgrading stacks (AR6; dark blue symbols), and the distance from the closest active surface oil sands mining, processing, or upgrading operation location (light blue symbols). The distance from the AR6 site between the two main upgrading stacks was historically used in the spatial analysis plots from the WBEA 2002 lichen study (Berryman et al., 2004), 2008 lichen study (Blum et al., 2012; Graney et al., 2012; Studabaker et al., 2012), and numerous other atmospheric deposition studies in the AOSR (Kelly et al., 2009; Kelly et al., 2010; Bari et al., 2014; Cho et al., 2014; Kirk et al., 2014; Fenn et al., 2015; Wieder et al., 2016).

Plots of metal concentrations versus minimum distance to a surface oil sands production facility (Appendix Table A.3) in most cases resulted in less variance and in all cases resulted in a shift in the exponential probability density function as a result of a larger scaling parameter (λ) versus plotting distance from the AR6 site. This finding suggests that proximity to surface mining, hauling, and upgrading operations and their associated coarse fugitive dust emissions were a major factor controlling inorganic element concentrations in lichens. In fact, when evaluating the concentrations of crustal elements (e.g., Al, Ca, La, Nb, U) as a function of distance to the closest oil sand production operation the spatial extent of the observed deposition impact appears to be 20–30 km rather than the 50–70 km zone of influence as interpreted

Table 2
Summary of Trace Elements in *H. physodes* Above the MDL (μg g^{-1}).

Analyte	MDL	n	Mean	Std Dev	Min	Q1	Median	Q3	Max
Total Sulfur (%)	20	127	0.107	0.030	0.070	0.086	0.101	0.121	0.285
Total Nitrogen (%)	200	127	0.695	0.173	0.480	0.570	0.630	0.770	1.585
Aluminum	1.46	127	2642.9	1785.5	708.5	1293.7	1926.3	3476.6	9050.4
Antimony	0.010	127	0.051	0.048	0.015	0.029	0.037	0.060	0.421
Arsenic	0.009	127	0.619	0.366	0.234	0.368	0.474	0.737	2.196
Barium	0.013	127	37.01	14.29	18.90	26.68	33.26	42.12	107.59
Beryllium	0.008	122	0.075	0.048	0.009	0.039	0.063	0.097	0.275
Bismuth	0.001	126	0.022	0.016	0.002	0.012	0.022	0.027	0.149
Cadmium	0.001	127	0.239	0.136	0.062	0.134	0.210	0.290	0.847
Calcium	17	127	15,818	12,974	2372	8414	12,187	18,591	92,735
Cerium	0.002	127	3.820	2.956	0.803	1.661	2.651	5.136	16.815
Cesium	0.001	127	0.242	0.117	0.076	0.156	0.212	0.299	0.649
Chromium	0.034	127	2.769	1.978	0.732	1.304	1.958	3.746	10.835
Cobalt	0.002	127	0.668	0.441	0.206	0.320	0.457	0.958	2.005
Copper	0.024	127	3.964	1.787	1.776	2.906	3.439	4.380	14.262
Iron	2.62	127	2148.3	1611.2	528.4	920.4	1532.1	2873.2	8374.2
Lanthanum	0.077	127	1.814	1.407	0.392	0.793	1.294	2.366	8.349
Lead	0.008	127	2.816	0.937	1.156	2.114	2.668	3.258	6.844
Lithium	0.005	127	1.589	1.343	0.235	0.552	1.105	2.365	7.185
Magnesium	0.522	127	821.9	297.6	441.2	592.1	745.4	982.4	2052.2
Manganese	0.014	127	191.28	104.88	63.25	119.99	159.38	241.77	672.40
Molybdenum	0.002	127	0.320	0.267	0.051	0.136	0.226	0.422	1.959
Neodymium	0.001	127	1.756	1.354	0.374	0.751	1.208	2.405	7.276
Nickel	0.120	127	4.470	2.840	1.432	2.291	3.207	6.156	15.402
Niobium	0.001	127	0.275	0.203	0.066	0.126	0.195	0.383	1.296
Palladium	0.001	81	0.044	0.060	0.003	0.015	0.031	0.049	0.457
Phosphorus	3.52	127	728.5	162.8	434.0	591.2	734.9	829.2	1247.6
Platinum	0.001	101	0.011	0.035	0.001	0.002	0.004	0.007	0.332
Potassium	1.21	127	3100.7	598.8	1973.3	2648.6	2979.0	3562.2	4768.1
Praseodymium	0.001	127	0.453	0.349	0.093	0.195	0.313	0.617	1.943
Rubidium	0.002	127	9.367	3.057	3.874	6.909	9.205	11.528	17.934
Samarium	0.001	127	0.339	0.266	0.065	0.138	0.228	0.466	1.314
Selenium	0.024	127	0.885	0.528	0.170	0.501	0.705	1.171	2.795
Silicon	55	127	6812	4385	1226	3704	5211	8741	23,528
Sodium	1.08	127	216.0	140.6	75.7	129.8	171.5	252.3	1014.1
Strontium	0.008	127	17.599	11.325	6.085	9.893	13.999	19.968	60.388
Tantalum	0.003	111	0.030	0.025	0.004	0.009	0.022	0.040	0.099
Thallium	0.002	127	0.038	0.017	0.007	0.025	0.034	0.047	0.107
Thorium	0.019	127	0.407	0.334	0.030	0.160	0.278	0.546	1.932
Tin	0.012	127	0.176	0.234	0.028	0.072	0.102	0.180	1.520
Titanium	0.194	127	87.35	63.10	18.63	41.12	63.31	118.61	345.05
Tungsten	0.002	127	0.157	0.178	0.012	0.042	0.082	0.217	1.028
Uranium	0.001	127	0.111	0.076	0.028	0.055	0.081	0.138	0.418
Vanadium	0.041	127	8.061	5.881	1.616	3.414	5.938	11.266	35.792
Zinc	0.254	127	46.56	9.72	32.07	39.48	43.85	51.84	95.57

from the lichen collection site distance to AR6 plots (Fig. 2; Appendix Fig. B.4). This finding is consistent with the observation that the near-field enhancement is due to coarse fugitive particulate emissions. Note in Fig. 2 that there are four high concentration "outliers" (from 90 to 140 km), which likely represent resuspended dust captured by lichens from some type of surface disturbance. This interpretation was verified through visual assessments of land use from satellite images (Appendix Fig. B.5).

Similar results to the inorganic element concentration relationships between sample location and distance to oil sand production operation were found with PAHs (e.g., Fig. 2; *H. physodes* concentration (ng g^{-1}; y- axis) and distance (km; x-axis)). This finding suggests proximity to oil sand production operation are the major factor determining PAH incorporation into *H. physodes* and is a better spatial reference point than the distance from the AR6 site. Plotting *H. physodes* concentration versus minimum distance to an active surface oil sands production operation also provides a good means of reference for comparative purposes in past and future studies as the number and location of mining operations change over time. The Fig. 2 outlier samples characterized by elevated crustal element concentrations in the southern portion of the study domain do not have similarly elevated PAH concentrations.

To support and supplement interpretations made from the concentration versus distance trends plots, kriged spatial interpolation plots were generated for a subset of the PAH and inorganic elements analytes to depict concentration gradients throughout the AOSR sampling domain. Spatial interpolation of concentration gradients for a selected crustal (Al) and an oil related (V) inorganic elements are plotted for comparison in Fig. 3a and b, respectively. High concentrations of crustal elements occur near the active surface oil sand production operations in the vicinity of Fort McKay, as well as at sites adjacent to the roadway network between Anzac and Conklin in an area containing in situ production sources. The oil sands production related elements also have high concentrations near the mining operations, but lower concentrations in the southern portion of the study domain in the vicinity of Conklin. This suggests resuspended fugitive dust from road ways, land clearing, and in situ bitumen production related infrastructure construction activities can be a major source of particulate emissions collected by *H. physodes* away from the surface oil sand mining operations. Spatial interpolation plots for PAH compounds phenanthrene and benzo (a) pyrene are depicted in Fig. 3c and d, respectively. The highest concentrations of PAH compounds in lichens occurs near the oil sands mining operations southeast and northwest of Fort McKay.

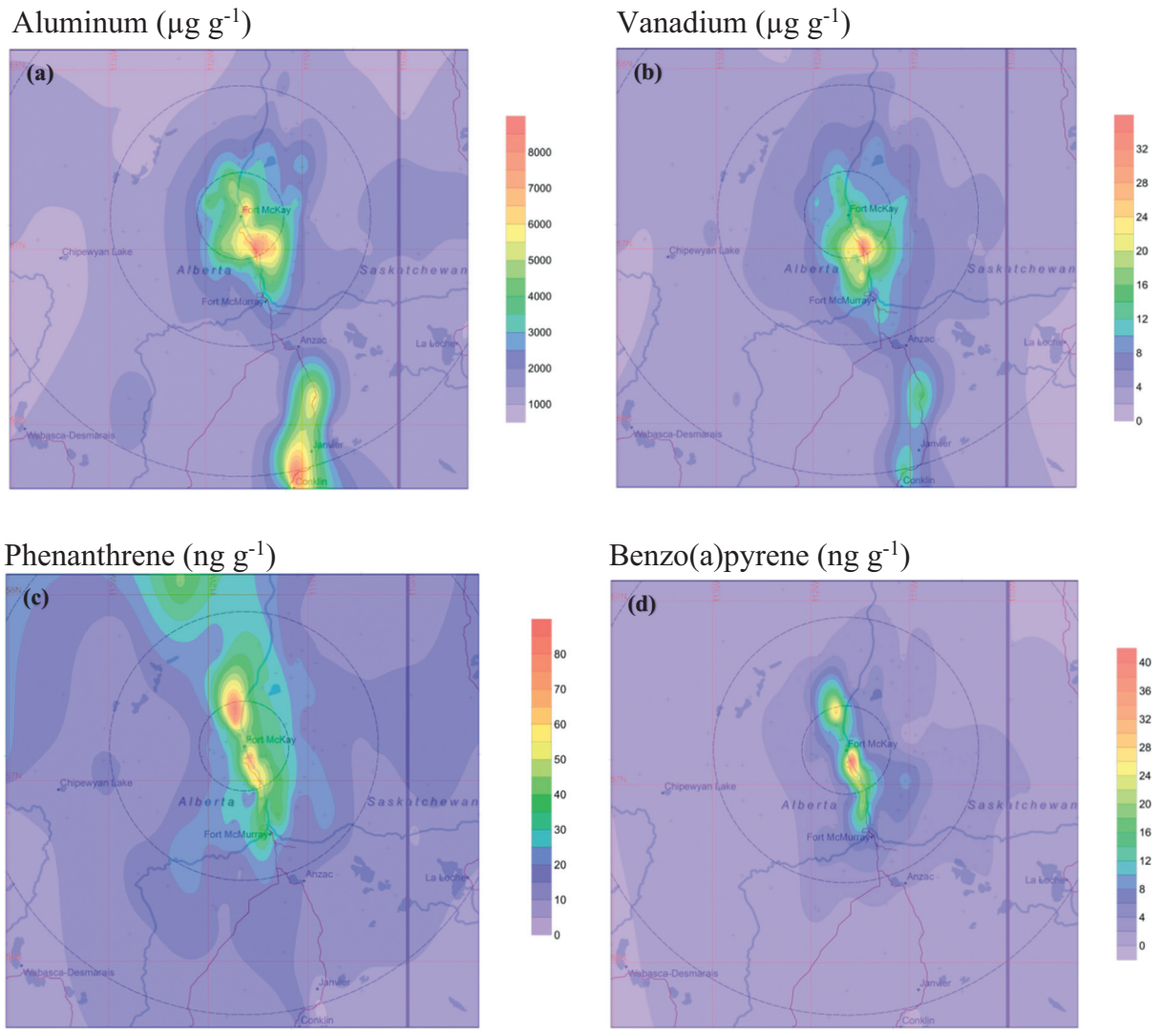

Fig. 3. Spatially Interpolated *H. physodes* Plots for Metals (top row) and PAHs (bottom row).

3.4. Source apportionment results

PMF model solutions generating from 6 to 9 factors were considered; with the final number chosen based on interpretability as well as stability across bootstrap-replicate data sets. The eight-factor solution was found to be optimal in terms of both explained variance and model fit statistics (Appendix Table A.9). An extremely low change in Q (−0.01%) and no factor swaps were observed with the displacement method using all 52 analytes for error analysis. Of the 100 bootstrap runs, all factors except "Upgrader Stack Emissions" (Factor 5) and "Raw Oil Sand" (Factor 8), were correctly mapped to their base factor in ≥98% of the runs. Upgrader Stack Emissions and Raw Oil Sand factors were mapped to their base factors in 74, and 82% of the runs, respectively, which were considered sufficiently stable after evaluating their spatial and temporal contribution trends. There were no rejected (unmapped) factors. The eight factor profiles obtained from the optimal PMF receptor modeling solution using all of the 127 lichen samples are presented in Fig. 4. Individual analyte concentrations in the profiles were considered significantly different from zero and included in the figure if the 5th percentile concentrations were >0. Profile concentrations, and the 5th and 95th percentile concentrations from the bootstrap runs are presented in Appendix Table A.10. All eight PMF factors yielded PI values <0.3, so use of a strictly "pyrogenic" descriptor for describing PI results may not be appropriate.

Overall, three local oil sand production related area fugitive dust sources (Petroleum Coke, Haul Road Dust, Raw Oil Sand), one local oil sand production related point source type (Upgrader Stack Emissions), and two local/regional area sources (Biomass Combustion, Mobile Source), were identified as contributing to the total lichen burden of PAHs and inorganic elements in the sampling domain. In addition, two lichen "biogeochemical" factors were identified that contain biogeochemically relevant elements and are hypothesized to reflect differences in lichen concentrations due to jack pine or black spruce host tree species influences and not emission source related atmospheric deposition. *H. physodes* hosted by black spruce in general have greater Mn, Zn, and Pb than jack pine at a similar distance from the mining operations. Lichens hosted by jack pine typically have greater Cd, Rb, and K than black spruce at a similar distance from the mining operations. These tree species dependencies probably reflect biogeochemical factors related to processes that are distinct from the source signatures of atmospheric wet and dry deposition from mining related activities. However, the incorporation of PAH compounds into *H. physodes* do not appear to be influenced by these processes.

3.4.1. Description of PMF model factors

3.4.1.1. PMF Factor 1 - manganese-biogeochemical. This factor is loaded with 61% and 26% of the measured Mn and Zn concentrations,

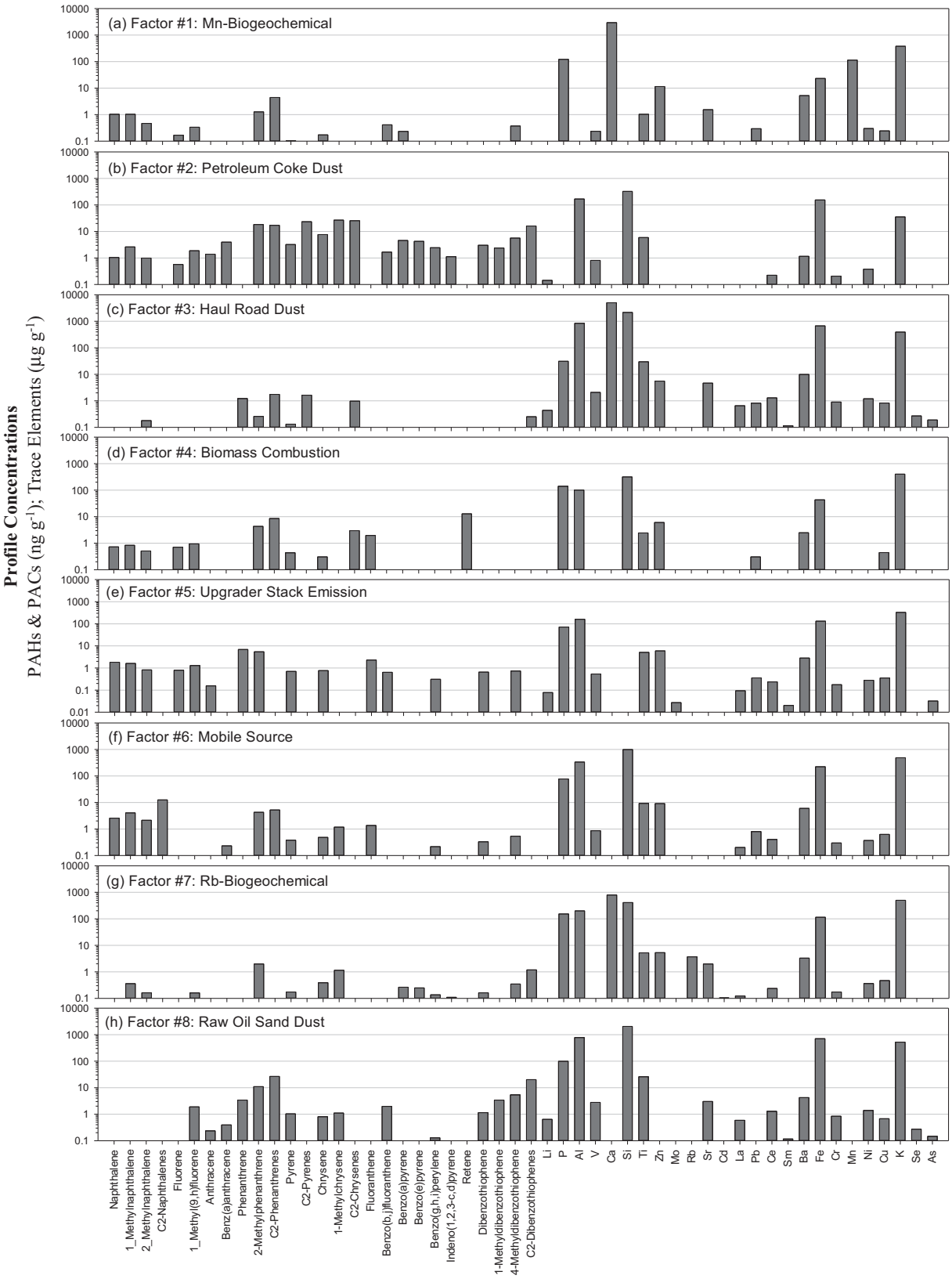

Fig. 4. PMF Model Factor Profiles of *H. physodes* Samples.

respectively. Naphthalene and C1- and C2-phenanthrenes are also found in appreciable concentrations in this factor. Overall, this factor explains 5% of the inorganic element and 4% of ΣPAH + PAC load. The spatial map of this factor contribution estimates (Fig. 5a) shows that Mn is depleted in close proximity to the main oil sand mining and production areas. Larger source contributions are observed at higher elevation sites, and minimal contributions are seen in samples collected in lower elevation areas. There is also a significant difference ($\alpha = 0.05$) between

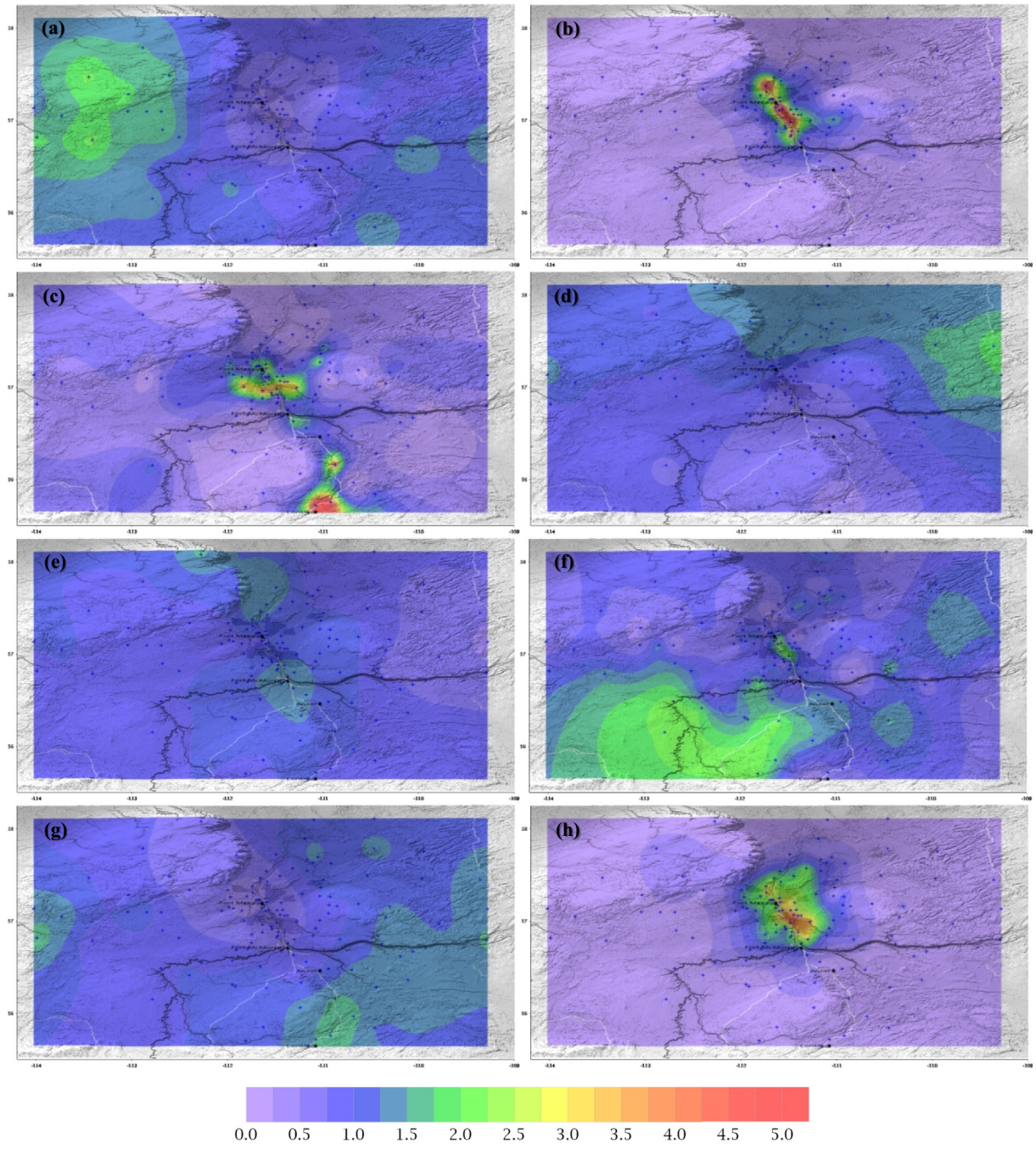

Fig. 5. Spatial Distribution of PMF Modeled Factor Source Contribution Estimates for (a) Mn-Biogeochemical, (b) Petroleum Coke Dust, (c) Haul Road Dust, (d) Biomass Combustion, (e) Upgrader Stack Emission, (f) Mobile Source, (g) Rb-Biogeochemical, and (h) Raw Oil Sand Dust.

mean source contributions of this factor in relation with the lichen host tree. *H. physodes* hosted by black spruce in general have greater Mn, Zn, and Pb than jack pine at a similar distance from the mining operations (Graney et al., 2012, Landis et al., 2012, and this study). Therefore, this factor is thought to represent a biogeochemical characteristic of *H. physodes* related to the black spruce host.

3.4.1.2. PMF Factor 2 - petroleum coke dust. The spatial distribution of contributions from Factor 2 (Fig. 5b) show only near field impact. At sites ~50 km away from the center of the mining operations contributions become insignificant. This observation constrains our assignment to oil sands production sources emitting large mass median aerodynamic diameter (MMAD) PM with a limited atmospheric residence time. Factor 2 is loaded with PAHs and PACs (~41% of ΣPAH + PAC loading), by far the largest contributor to atmospheric deposition than any of any of the identified source factors. In contrast to the ΣPAH + PAC, only 7% of the inorganic element load is found in this factor (Fig. 6c). The PAH and PAC profile of each factor was evaluated by calculating the ratio of each component to the sum of all PAHs and PACs used to calculate the modified PI and compared to reported profiles for petroleum coke and ore (Jariyasopit et al., 2018). The Factor 2 PAH and PAC analyte profile is consistent with that of petroleum coke ($r^2 = 0.56–0.58$), and gave a modified PI of 0.17, which suggests a primarily non-petrogenic source. Retene and crustal elements are largely absent from this factor. Elements associated with local sources including vehicular exhaust emissions, petroleum products, and bitumen (e.g., V and Ni) are present

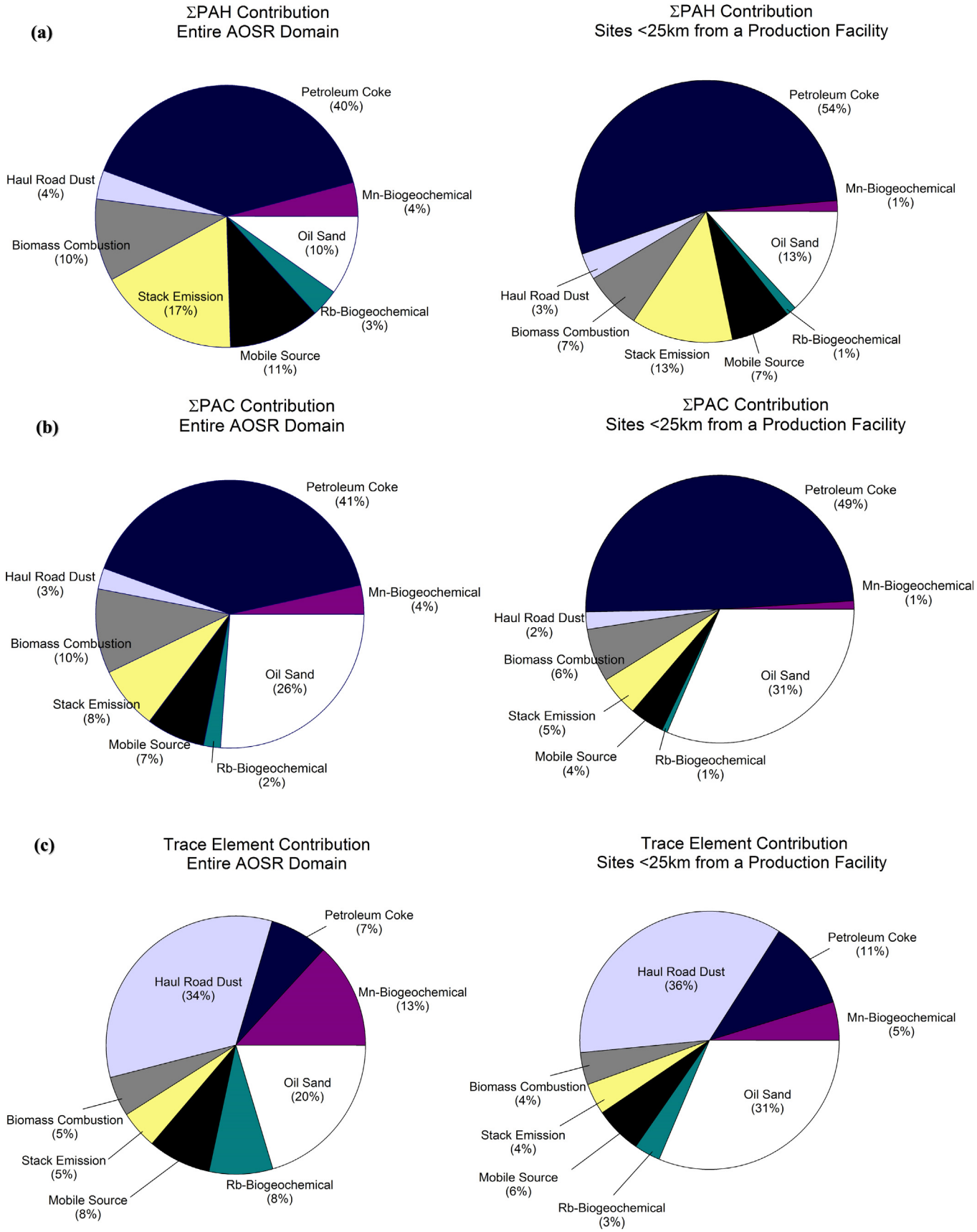

Fig. 6. PMF Mass Apportionment of (a) ΣPAH, (b) ΣPAC, and (c) Trace Elements for the Entire Study Domain and within 25 km of a Primary Surface Oil Sand Production Facility.

but relatively minimal. Large stockpiles of petroleum coke from bitumen upgrading are found near upgrader locations in the AOSR (Appendix Fig. B.1) and are susceptible to wind erosion.

3.4.1.3. PMF Factor 3 - haul road dust. High loading of inorganic elements such as Ca, Sr, and Ba characterize this factor. Landis et al. (2012) documented inorganic abundances of elements in source materials from AOSR including haul road dust, tailing sand, petroleum coke, oil sand and bitumen. Of all the materials studied, Ca was found at the highest concentration in haul road dust. This factor also contains the highest loading of crustal elements such as Si, Ce, Ti, Cr, Al, and Fe, further strengthening the assignment of this factor to haul road fugitive dust emissions. The limestone mined in the AOSR underlying the oil sand deposits is used in constructing temporary roads for truck hauling operations and is the likely source of the elevated Ca concentrations in this factor. Spatial contribution estimates presented in Fig. 5c show high loadings near the central oil sands mining area, and further south along a roadway where unpaved roads and parking areas supporting logging and land clearance activities are ongoing for in situ production operations (Appendix Fig. B.5). Approximately 34% of the inorganic elements but only 3% of ΣPAH + PAC are loaded on this factor.

3.4.1.4. PMF Factor 4 – biomass combustion. This factor accounts for 10% of both the modeled ΣPAHs and ΣPACs and is dominated by low molecular weight PAHs and PACs. Factor 4 also accounts for 100% of retene, a commonly measured softwood combustion marker. The fluoranthene/pyrene ratio of 4.5 contrasts with the ratios of 0.4–0.9 measured for petroleum coke and ore. All of these are suggestive of sources associated with biomass burning (Stogiannidis and Laane, 2015). Landis et al. (2017) highlighted the substantial impact of repeated wildfire smoke events on measured $PM_{2.5}$ concentrations in the Fort McKay community in 2011, 2012, 2014, and 2015. The alkyl DBTs, which are found in the oil sands source materials as well as diesel fuel and diesel exhaust, are absent from this factor. Significant loadings of inorganic tracers consistent with biomass combustion such as K, P, and Zn are also found on this factor. Graney et al. (2012) and Landis et al. (2012, 2017) found Cd as a unique elemental tracer for AOSR wildfire emissions. However, Cd is not loaded on this factor, rather it is loaded on Factor 7 (the Rb – Biogeochemical factor which is associated with jack pines, a boreal forest species prone to wildfire loss in the AOSR). Spatially this factor is prevalent in the northeast portion of the sampling domain (Fig. 5d), and 5% of the inorganic elements and 10% of ΣPAH + PAC are loaded onto this factor.

3.4.1.5. PMF Factor 5 – upgrader stack emission. Spatially, this factor aligns with low elevations along the Athabasca River Valley, north and south of most of the surface mining operations (Fig. 5e). This spatial distribution pattern is suggestive of emissions into the river valley with flows through the drainage basin. Approximately 5% of the inorganic elements, 8% of ΣPACs, and 17% of the ΣPAHs are loaded on this factor. Tentatively we identify this factor as stack emissions, due to its spatial distribution and relatively lower loadings of ΣPAH + ΣPAC (10%) compared to Factors 2 (Petroleum Coke) and 8 (Raw Oil Sand). The profile does not resemble either Petroleum Coke or Raw Oil Sand sources (r^2 < 0.02). Other molecular indices for source attribution paint an ambiguous picture (e.g., modified PI = 0.2 - similar to petroleum coke); fluoranthene/pyrene = 3.2 (more pyrogenic). Abundances of PAH/PACs in stack emissions from the AOSR have been found to be low compared to those in the petroleum coke dust and diesel samples (Wang et al., 2015). In aggregate upgrader stacks in the AOSR have been found to release perylene, dibenzothiophene, benz(a)anthracene, and chrysene, as the most abundant components as well as 1 methyl phenanthrene, 9-fluorenone, and pyrene (Harner et al., 2018) which load into this factor. More information about PAH and PAC from AOSR stack emissions, their transformation and deposition fields are needed to confirm this factor source designation.

3.4.1.6. PMF Factor 6 - mobile source. Lower molecular weight PAHs dominate in this factor. This factor accounts for 7% of ΣPACs and 11% of ΣPAHs, is not consistent with known oil sands source profiles, and molecular indices were ambiguous (modified PI = 0.07, petrogenic; fluoranthene/pyrene = 3.6, pyrogenic). C1- and C2-naphthalenes are virtually absent from raw oil sand but are produced during upgrading and are found in both petroleum coke and upgraded synthetic crude (Yang et al., 2011; Jariyasopit et al., 2016). The lower molecular weight alkyl-PAH abundances tend to increase with upgrading in these samples, with the sweet blend, a precursor for diesel fuel that is sometimes added to the mine fleet fuel, containing substantial amounts of naphthalene derivatives. Zn and Pb are two inorganic tracers present in this factor that are also indicative of vehicular emissions (Reff et al., 2007).

Wang et al. (2015, 2016) measured average abundances of particle and vapor phase PAHs in various sources such as mine overburden, unpaved road, tailings pond dikes, coke piles, upgrader stacks, and fleet emissions from the AOSR region. They found that fleet vehicles emitted substantial amounts of PAHs and PACs, and emission signatures were consistent with diesel exhaust emissions elsewhere. Spatial distribution of the factor source contribution estimates (Fig. 5f) suggest that this factor likely represents local (centered over the oil sands operations) and regional emissions (southwest portion of sampling domain) from vehicle combustion related activities. This spatial pattern indicates that gas to coarse particle adsorption and/or gas phase uptake of PACs by *H. physodes* may be an important contributor to lichen burden since mobile source emissions are in the form of fine and ultrafine particles, and consequently have atmospheric residence times ranging from days to weeks.

3.4.1.7. PMF Factor 7 – rubidium – biogeochemical. Much like the Mn dominated biogeochemical factor, the spatial map of this factor's source contribution estimates (Fig. 5g) shows *H. physodes* concentrations are lower in close proximity to the main oil sand mining and production areas. However, this factor is unique in terms of the presence of Rb and Cd. Though minimal, some parent PAH analytes are present, and C1-phenanthrenes and C1-chrysenes are also found. Approximately 8% of the inorganic elements and 3% of Σ PAH + PAC are loaded on this factor. *H. physodes* hosted by jack pine typically have greater Cd, Rb, and K than black spruce at a similar distance from the mining operations (Graney et al., 2012; Landis et al., 2012). Therefore, this factor is thought to represent a biogeochemical characteristic of *H. physodes* related to the jack pine host.

3.4.1.8. PMF Factor 8 – raw oil sand dust. This factor is characterized by high loadings in PACs (26% of ΣPACs across all factors) relative to PAHs (10%). This contrasts with 41% and 41%, respectively, in Factor 2, and 8% and 17% in Factor 5. The modified PI for Factor 8 is 0.05. The most enriched elements in bitumen such as Mo, V, Ni are also heavily loaded in this factor, along with crustal elements such as Si, Al, La, Ce, Sm, Ba, Ti, and Cr (Landis et al., 2012).

Recent analyses of petroleum coke from delayed and fluid processes showed that PACs are depleted relative to PAHs in comparison to the original ore from which they are derived (Jariyasopit et al., 2018; Harner et al., 2018). Although source sample data are available only for a small number of samples (5 total petroleum coke and 3 raw oil sand ore), the PAC depletion was particularly evident for the dibenzothiophenes, for which the ratio (C1 + C2 DBTs)/DBT in ore (44.3) was 10-fold higher than in petroleum coke (4.46–4.84). Applying this ratio to the PMF data, we find that Factor 8 yields a value of 25.2, whereas all other factors yield a value <10. Coupled with the modified PI of <0.10, this suggests a mainly petrogenic origin for Factor 8, with little contribution from petroleum coke or pyrogenic sources. The spatial footprint for this factor is centered over the mining operations (Fig. 5h) and has a greater spatial extent than Factor 2 (Petroleum Coke). This source is thought to represent a ground level wind-blown coarse particle fugitive dust emission of raw oil sand ore generated by

mechanical shovel and hauling operations. Overall, 20% of the inorganic elements and 22% of ΣPAH + PAC are loaded on this factor.

3.4.2. H. physodes mass apportionment

The major goals of this source apportionment modeling study were to elucidate the spatial deposition pattern of PAHs in the AOSR, and to quantify the contributing emission source types (Fig. 6a). ΣPAH + PAC in *H. physodes* in the AOSR ranged from 54 to 2778 ng g^{-1} with a median concentration of 317 ng g^{-1}. The contribution of each factor or source type to *H. physodes* composition was quantitatively assessed by means of multiple linear regression. Using source contribution estimates from PMF as independent variables, MLR analyses were conducted with ΣPAH + PACs, ΣPAH, ΣPAC, total nitrogen, total sulfur, and metals load as dependent variables.

The MLR run with ΣPAH + PAC exhibited an adjusted coefficient of determination of 0.99 ($p < 0.0001$), explaining 99% of the ΣPAH + PAC variance. Appendix Fig. B.6 presents a comparison of the predicted ΣPAH + PAC concentrations, calculated from the model parameter estimates against measured ΣPAH + PAC. All eight factors showed significant contributions (at $\alpha = 0.05$) to the measured ΣPAH + PAC. The Petroleum Coke factor accounts for 41% of the ΣPAH + PAC load. The Raw Oil Sand factor is the second largest ΣPAH + PAC source (22%). Biomass Combustion, Stack Emissions, Mobile Sources, Haul Road Dust, Mn-biogeochemical, and Rb-biogeochemical sources account for 10, 10, 8, 3, 4, and 3% of the Σ PAH + PACs, respectively.

ΣPAC contribution estimates to individual sources are approximately 1.8–11.3 times higher than the contribution estimates calculated for ΣPAH. The lowest ΣPAC/ΣPAH ratio corresponds to the Upgrader Stack Emissions factor. This result is consistent with a high temperature combustion processes that is expected to produce unsubstituted PAHs. The highest ΣPAC/ΣPAH ratio (11.3) is observed for the Raw Oil Sand factor, which is also in line with expectations for a source with petrogenic origins. The Petroleum Coke factor exhibits a ΣPAC/ΣPAH ratio of 4.3.

The impact of oil sand production operations to the surrounding AOSR sampling domain was explored on the basis of distance to the closest oil sand production operation. Contributions of ΣPAH + PAC to *H. physodes* collected within 25 km, between 25 and 50 km, 50–100 km, and > 100 km radius were analyzed (Appendix Fig. B.7). Significant contributions from the Petroleum Coke and Raw Oil Sand fugitive dust sources extended up to a distance of 50 km and became negligible (<10 ng g^{-1}) beyond 100 km from known oil sand production operations. The Upgrader Stack Emissions, Biomass Combustion, and Mobile Sources factors, whose emissions are dominated by fine and ultrafine particles, do not exhibit distinct spatial trends. Their source contributions were similar at all distance increments. The Haul Road Dust factor shows appreciable near field ΣPAH + PAC (21 ng g^{-1}) consistent with the unpaved road infrastructure associated with oil sand production operations, contributions lessen beyond 25 km.

The sources of ΣPAH (Fig. 6a) and ΣPAC (Fig. 6b) in *H. physodes* collected within 25 km of a surface oil sand production operation were further investigated to highlight the relative importance of specific near-field impacts of mining and upgrading source types on atmospheric deposition of PAHs to *H. physodes*. A total of 56*H. physodes* samples were collected within 25 km of a surface oil sand mining or upgrading facility. Fig. 6a, b, and c present apportioned ΣPAH, ΣPAC, and Σmetals for the entire study domain ($n = 127$) and within 25 km of an active surface oil sand production facility. In the near-field sampling domain (25 km), Petroleum Coke contributed 13.8% more ΣPAH, 8.4% ΣPAC, and 3.9% total metals in comparison with the entire study domain on a relative mass basis. Similarly, a 3.3% increase of ΣPAH, a 5.3% ΣPAC and 11% of total metals were observed for Raw Oil Sand. These two sources account for 63% of ΣPAH + PAC emissions from the entire study region ($n = 127$). Out of this 63% (43.2 μg g^{-1}), up to 90% (39.9 μg g^{-1}) ΣPAH + PAC emissions are found within 25 km from a surface oil sand production operation. Regional sources (Biomass Combustion and Mobile Sources) account for 19% of ΣPAH + PAC emissions from the entire study region, of which 46% were found to originate from near-field operations. This outcome further confirms that coarse fraction particle atmospheric deposition from fugitive dust is the dominant source of ΣPAH + PAC in the vicinity of oil sand production operations.

Interest in the atmospheric deposition total nitrogen and total sulfur with relatively high regional emission rates and their potential direct and indirect ecological impacts (e.g., plant toxicity, soil acidification, eutrophication) lead us to investigate their contributing sources (Foster et al., 2019). Overall, the 8-Factor PMF model MLR analysis explained 74 and 63% of the measured total nitrogen and total sulfur, respectively. The relatively large unexplained mass may represent gas phase absorption of SO_x and NO_x by *H. physodes*. Of the explained mass, Raw Oil Sand, Biomass Combustion, Upgrader Stack Emissions, and Mobile Sources accounted for 23, 14, 10, and 19% of total sulfur, and 14, 25, 13, and 21% of total nitrogen, respectively. The Rb-Biogeochemical factor had 6–7 times higher total nitrogen (14 versus 2%) and total sulfur (13 versus 2%) loading compared to the Mn Biogeochemical factor.

4. Conclusions

This study represents the most extensive epiphytic lichen bioindicator study to date that has coupled the measurement of PAHs, PACs, and inorganic elements in the AOSR from an integrated source apportionment perspective. The EPA PMF5.1 receptor model was applied to the comprehensive study analytical data set and used to identify eight major source factors that contribute to the PAH, PAC, and inorganic elements incorporated into *H. physodes* in the AOSR sampling domain. These included four anthropogenic oil sands production related sources (Petroleum Coke, Haul Road Dust, Stack Emissions, Raw Oil Sand), two local/regional sources (Biomass Combustion, Mobile Source), and two biogeochemical source types related to host tree species. Source identification was refined and improved from prior lichen-based studies in the AOSR through incorporation of PAH and PAC analytes. On average, 99% of the measured ΣPAH + PAC *H. physodes* concentrations were explained by the 8-factor PMF model. Fugitive Petroleum Coke and Raw Oil Sand dust were identified as the major sources of ΣPAH + PAC deposition in the AOSR. These two sources accounted for 63% (43.2 μg g^{-1}) of ΣPAH + PAC deposition to the entire study domain. Of this overall 43.2 μg g^{-1} contribution, approximately 90% (39.9 μg g^{-1}) ΣPAH + PAC was deposited within 25 km of the closest surface oil sand production facility. Regional sources (Biomass Combustion and Mobile Sources) accounted for 19% of ΣPAH + PAC deposition to the entire study domain, of which 46% was deposited near-field to oil sand production operations.

The petroleum coke fugitive dust source identified in this study was not apparent in a previous 2008 AOSR lichen collection and inorganic analyte source apportionment study (Landis et al., 2012) and highlights the importance of including PAHs and PAC tracer analytes in source apportionment studies. The Petroleum Coke factor identified in this study explains the majority of the ΣPAHs and ΣPACs in the AOSR (41%) in this analysis, but only explains 7% of the trace element loading. This dichotomy in the source signature, highlights the difficulty in identifying the petroleum coke signal when only utilizing inorganic parameters in the PMF receptor model. The epiphytic lichen bioindicator results from this study are consistent with other recent studies that identified the importance of fugitive petroleum coke dust to near field PAH atmospheric loadings from the oil sand production operations in the AOSR (Jautzy et al., 2015; Zhang et al., 2016; Manzano et al., 2017), particularly from coke pile storage activities adjacent to the Athabasca River.

Use of data analysis techniques including plots of *H. physodes* concentration versus distance to sources, spatially interpolated *H. physodes* concentrations, and satellite imagery allowed for the elucidation of both the location of atmospheric deposition enhancement zones as well as the areal extent of various oil sands mining operation emissions have on PAH, PAC, and metals deposition gradients. The

surface disturbance processes can be a major source of fugitive dust emissions and can be recognized in *H. physodes* by their enhanced crustal element concentrations and absence of PAH and PAC compounds. The spatial scale of emissions from surface oil sand production operations on PAH, PAC, and inorganic element incorporation within *H. physodes* was best determined by use of a minimum distance metric to all major surface oil sand production operations, reducing the effective extent of the fugitive dust impacts to a distance of ~25 km. This is a conceptual improvement from prior studies using the AR6 site between the two longest-operating upgrading stacks and suggests that surface mining operations and the generation of fugitive dust are the main factors related to the highest PAH, PAC, and inorganic concentration levels in lichens.

Acknowledgements

This work was funded by the Wood Buffalo Environmental Association (WBEA), Fort McMurray, Canada, contract Number AA108-17. The content and opinions expressed by the authors do not necessarily reflect the views of the WBEA or of the WBEA membership. We thank Kevin Percy (WBEA) for managing the lichen collection activities in the AOSR; Natalie Bonnell, Abigale Glashoerster, Asad Hidayat, and Evan Magill (WBEA) for lichen collection and cleaning support; pilots Carry Zimmer and Tyler Kahret (Lakeshore Helicopters); Joel Blum (University of Michigan) for inorganic lichen sample grinding; Mike Fort (ARA) lichen extraction and DRC-ICPMS analysis; Keith Briggs (RTI) for organic lichen component extraction and cleanup; Michelle McCombs and Cynthia Salmons (RTI) for lichen TOF analysis and TOF data QA review, respectively. This paper is dedicated to the memory of Dr. Keith Puckett.

Appendix A. Supplementary data

Supplementary data to this article can be found online at https://doi.org/10.1016/j.scitotenv.2018.11.131.

References

Ahad, J.M., Gammon, P.R., Gobeil, C., Jautzy, J., Krupa, S., Savard, M.M., Studabaker, W.B., 2014. Evaporative emissions from tailings ponds are not likely an important source of airborne PAHs in the Athabasca oil sands region. Proc. Natl. Acad. Sci. U. S. A. 111, E2439.

Ahad, J.M.E., Jautzy, J.J., Cumming, B.F., Das, B., Laird, K.R., Sanei, H., 2015. Sources of polycyclic aromatic hydrocarbons (PAHs) to northwestern Saskatchewan lakes east of the Athabasca Oil Sands. Org. Geochem. 80, 35–45.

Alberta Energy, 2017. Energy: Annual Report 2016–2017. Government of Alberta, June 2017. ISBN 1703-4582. https://open.alberta.ca/dataset/cbd7147b-d304-4e3e-af28-78970c71232c/resource/7f360403-7e80-40c9-8f7a-0a5079d14f55/download/2016-17-Annual-Report-Energy.pdf. Last Accessed October 19, 2018.

Alberta Energy Regulator, ST98, 2017. Alberta's Energy Reserves & Supply/Demand Outlook. Government of Alberta, March 2017. https://www.aer.ca/providing-information/data-and-reports/statistical-reports/st98, Accessed date: 19 October 2018.

Bari, M.A., Kindzierski, W.B., Cho, S., 2014. A wintertime investigation of atmospheric deposition of metals and polycyclic aromatic hydrocarbons in the Athabasca Oil Sands Region, Canada. Sci. Total Environ. 485–486, 180–192.

Berryman, S., Geiser, L.H., Brenner, G., 2004. Depositional Gradients of Atmospheric Pollutants in the Athabasca Oil Sands Region, Alberta, Canada: An Analysis of Lichen Tissue and Lichen Communities. Lichen Indicator Pilot Program 2002–2003. Report Prepared for the Wood Buffalo Environmental Association, Fort McMurray, AB, Canada p. 171.

Berryman, S., Straker, J., Krupa, S., Davies, M., Ver Hoef, J., Brenner, G., 2010. Mapping the Characteristics of Air Pollutant Deposition Patterns in the Athabasca Oil Sands Region Using Epiphytic Lichens as Bioindicators. Interim Report Submitted to the Terrestrial Environmental Effects Monitoring (TEEM) Science Sub-committee of the Wood Buffalo Environmental Association, Fort McMurray, AB, Canada.

Birks, S.J., Cho, S., Taylor, E., Yi, Y., Gibson, J.J., 2017. Characterizing the PAHs in surface waters and snow in the Athabasca region: Implications for identifying hydrological pathways of atmospheric deposition. Sci. Total Environ. 603–604, 570–583.

Blum, J.D., Johnson, M.W., Gleason, J.D., Demers, J.D., Landis, M.S., Krupa, S., 2012. Mercury concentration and isotopic composition of epiphytic tree lichens in the Alberta Oil Sands Region. In: Percy, Kevin (Ed.), Alberta Oil Sands: Energy, Industry and the Environment. Elsevier, Oxford, England.

Boutin, C., Carpenter, D.J., 2017. Assessment of wetland/upland vegetation communities and evaluation of soil-plant contamination by polycyclic aromatic hydrocarbons and trace metals in regions near oil sands mining in Alberta. Sci. Total Environ. 576, 829–839.

Bytnerowicz, A., Hsu, Y.M., Percy, K., Legge, A., Fenn, M.E., Schilling, S., Fraczek, W., Alexander, D., 2016. Ground-level air pollution changes during a boreal wildland mega-fire. Sci. Total Environ. 572, 755–769.

Cho, S., Sharma, K., Brassard, B.W., Hazewinkel, R., 2014. Polycyclic aromatic hydrocarbon deposition in the snowpack of the Athabasca Oil Sands Region, Alberta, Canada. Water Air Soil Pollut. 225 (5), 1910.

Edgerton, E.S., Fort, J.M., Baumann, K., Graney, J.R., Landis, M.S., Berryman, S., Krupa, S., 2012. Method for extraction and multi-element analysis of *Hypogymnia physodes* samples from the Athabasca Oil Sands Region. In: Percy, Kevin (Ed.), Alberta Oil Sands: Energy, Industry and the Environment. Elsevier, Oxford, England, pp. 315–342.

Fenn, M.E., Bytnerowicz, S.L., Schilling, C.S., Ross, C.S., 2015. Atmospheric deposition of nitrogen, sulfur and base cations in jack pine stands in the Athabasca Oil Sands Region, Alberta, Canada. Environ. Pollut. 196, 497–510.

Foster, K.R., Davidson, C., Spink, D., 2019. Monitoring ecological responses to air quality and deposition in the Athabasca Oil Sands Region: the Wood Buffalo Environmental Association's terrestrial environmental effects monitoring program. Sci. Total Environ. (in review).

Garty, J., 2001. Biomonitoring atmospheric heavy metals with lichens: theory and application. Crit. Rev. Plant Sci. 20 (4), 309–371.

Graney, J.R., Landis, M.S., Krupa, S., 2012. Coupling lead isotopes and element concentrations in epiphytic lichens to track sources of air emissions in the Athabasca Oil Sands Region. In: Percy, Kevin (Ed.), Alberta Oil Sands: Energy, Industry and the Environment. Elsevier, Oxford, England, pp. 343–372.

Graney, J.R., Landis, M.S., Puckett, K.J., Studabaker, W., Edgerton, E.S., Legge, A., Percy, K.E., 2017. Differential accumulation of PAHs, elements, and Pb isotopes by five lichen species from the Athabasca oil sands region in Alberta, Canada. Chemosphere 184, 700–710.

Harner, T., Rauert, C., Muir, D., Schuster, J., Hsu, Y.M., Zhang, L., Marson, G., Watson, J.G., Ahad, J., Cho, S., Jariyasopit, N., Kirk, J., Korosi, J., Landis, M.S., Martin, J., Zhang, Y., Fernie, K., Wentworth, G.R., Wnorowski, A., Dabek, E., Charland, J.R., Pauli, B., Wania, F., Galarneau, E., Cheng, I., Makar, P., Whaley, C., Chow, J.C., Wang, X., 2018. Air synthesis review on polycyclic aromatic compounds in the Oil Sands Region. Environ. Rev. https://doi.org/10.1139/er-2018-0039 (in press).

Henry, R.C., Lewis, C.W., Hopke, P.K., Williamson, H.J., 1984. Review of receptor model fundamentals. Atmos. Environ. 18 (8), 1507–1515.

Hopke, P.K., 2009. Theory and application of atmospheric source apportionment. In: Legge, A.H. (Ed.), Air Quality and Ecological Impacts. Elsevier, Amsterdam, the Netherlands.

Hopke, P.K., 2016. A review of receptor modeling methods for source apportionment. J. Air Waste Manage. Assoc. 66, 237–259.

Jalkanen, L.M., Häsänen, E.K., 1996. Simple method for the dissolution of atmospheric aerosol samples for analysis by inductively coupled plasma mass spectrometry. J. Anal. At. Spectrom. 11, 365–369.

Jariyasopit, N., Harner, T., Wu, D., Williams, A., Halappanavar, S., Su, K., 2016. Mapping indicators of toxicity for polycyclic aromatic compounds in the atmosphere of the Athabasca Oil Sands Region. Environ. Sci. Technol. 50, 11282–11291.

Jariyasopit, N., Zhang, Y., Martin, J.W., Harner, T., 2018. Comparison of polycyclic aromatic compounds in air measured by conventional passive and passive dry deposition samplers and contributions from petcoke and oil sands ore. Atmos. Chem. Phys. Discuss. 18, 9161–9171. https://www.atmos-chem-phys.net/18/9161/2018/ (in review).

Jautzy, J.J., Ahad, J.M., Hall, R.I., Wiklund, J.A., Wolfe, B.B., Gobeil, C., Savard, M.M., 2015. Source Apportionment of Background PAHs in the Peace-Athabasca Delta (Alberta, Canada) Using Molecular Level Radiocarbon Analysis. Environ. Sci. Technol. 49, 9056–9063.

Jeran, Z., Jacimovic, R., Batic, F., Mavsar, R., 2002. Lichens as integrating air pollution monitors. Environ. Pollut. 120, 107–113.

Kelly, E.N., Short, J.W., Schindler, D.W., Hodson, P.V., Ma, M., Kwan, A.K., Fortin, B.L., 2009. Oil sands development contributes polycyclic aromatic compounds to the Athabasca River and its tributaries. Proc. Natl. Acad. Sci. U. S. A. 106, 22346–22351.

Kelly, E.N., Schindler, D.W., Hodson, P.V., Short, J.W., Radmanovich, R., Neilson, C.C., 2010. Oil sands development contributes elements toxic at low concentrations to the Athabasca River and its tributaries. Proc. Natl. Acad. Sci. U. S. A. 107, 16178–16183.

Kirk, J.L., Muir, D.C.G., Gleason, A., Wang, X., Lawson, G., Frank, R.A., Lehnherr, I., Wrona, F., 2014. Atmospheric deposition of mercury and methylmercury to landscapes and waterbodies of the Athabasca Oil Sands Region. Environ. Sci. Technol. 48, 7374–7383.

Korosi, J.B., Cooke, C.A., Eickmeyer, D.C., Kimpe, L.E., Blais, J.M., 2016. In-situ bitumen extraction associated with increased petrogenic polycyclic aromatic compounds in lake sediments from the Cold Lake heavy oil fields (Alberta, Canada). Environ. Pollut. 218, 915–922.

Kurek, J., Kirk, J.L., Muir, D.C.G., Wang, X., Evans, M.S., Smol, J.P., 2013. Legacy of a half century of Athabasca oil sands development recorded by lake ecosystems. Proc. Natl. Acad. Sci. U. S. A. 110, 1761–1766.

Landis, M.S., Pancras, J.P., Graney, J.R., Stevens, R.K., Percy, K.E., Krupa, S., 2012. Receptor modeling of epiphytic lichens to elucidate the sources and spatial distribution of inorganic air pollution in the Athabasca Oil Sands Region. In: Percy, Kevin (Ed.), Alberta Oil Sands: Energy, Industry and the Environment. Elsevier, Oxford, England, pp. 427–467.

Landis, M.S., Pancras, J.P., Graney, J.R., White, E.M., Edgerton, E.S., Legge, A., Percy, K.E., 2017. Source apportionment of ambient fine and coarse particulate matter at the Fort McKay community site, in the Athabasca Oil Sands Region, Alberta, Canada. Sci. Total Environ. 584–585, 105–117.

Landis, M.S., Kamal, A.S., Edgerton, E.S., Wentworth, G., Sullivan, A.P., Dillner, A.M., 2018. The impact of the 2016 Fort McMurray Horse River Wildfire on Ambient Air Pollution

Levels in the Athabasca Oil Sands Region, Alberta. Canada. Sci. Total Environ. 618, 1665–1676.
Lundin, J.I., Riffell, J.A., Wasser, S.K., 2015. Polycyclic aromatic hydrocarbons in caribou, moose, and wolf scat samples from three areas of the Alberta oil sands. Environ. Pollut. 206, 527–534.
Manzano, C.A., Marvin, C., Muir, D., Harner, T., Martin, J., Zhang, Y.F., 2017. Heterocyclic Aromatics in Petroleum Coke, Snow, Lake Sediments, and Air Samples from the Athabasca Oil Sands Region. Environ. Sci. Technol. 51, 5445–5453.
Masliyah, J., Zhou, Z., Xu, Z., Czarnecki, J., Hamza, H., 2004. Understanding water-based bitumen extraction from Athabasca Oil Sands. Can. J. Chem. Eng. 82, 628–654.
Osacky, M., Geramian, M., Ivey, D.G., Liu, Q., Etsell, T.H., 2013. Mineralogical and chemical composition of petrologic end members of Alberta Oil Sands. Fuel 113, 148–157.
Paatero, P., 1999. The multilinear engine - a table-driven least squares program for solving multilinear problems, including the n-way parallel factor analysis model. J. Comput. Graph. Stat. 8, 854–888.
Park, S.E., Henry, R.C., Spiegelman, C.H., 2000. Estimating the number of factors to include in a high-dimensional multivariate bilinear model. Commun. Stat. Simul. Comput. 29 (3), 723–746.
Polissar, A.V., Hopke, P.K., Paatero, P., Malm, W.C., Sisler, J.F., 1998. Atmospheric aerosol over Alaska 2. Elemental composition and source. J. Geophys. Res. 103, 19045–19057.
Ramdahl, T., 1983. Retene – a molecular marker of wood combustion in ambient air. Nature 306, 580–582.
Reff, A., Eberly, S.I., Bhave, P.V., 2007. Receptor modeling of ambient particulate matter data using positive matrix factorization: review of existing methods. J. Air Waste Manag. Assoc. 57, 146–154.
Schauer, J.J., Rogge, W.F., Hildemann, L.M., Mazurek, M.A., Cass, G.R., 1996. Source apportionment of airborne particulate matter using organic compounds as tracers. Atmos. Environ. 30, 3837–3855.
Schindler, D.W., 2014. Unravelling the complexity of pollution by the oil sands industry. Proc. Natl. Acad. Sci. U. S. A. 111, 3209–3210.
Schuster, J.K., Harner, T., Su, K., Mihele, C., Eng, A., 2015. First results from the oil sands passive air monitoring network for polycyclic aromatic compounds. Environ. Sci. Technol. 49, 2991–2998.
Simoneit, B.R.T., 2002. Biomass burning – a review of organic tracers for smoke from incomplete combustion. Appl. Geochem. 17, 129–162.
Stogiannidis, E., Laane, R., 2015. Source characterization of polycyclic aromatic hydrocarbons by using their molecular indices: an overview of possibilities. In: Whitacre, D. (Ed.), Reviews of Environmental Contamination and Toxicology. Reviews of Environmental Contamination and Toxicology (Continuation of Residue Reviews). Vol 234. Springer, Cham.
Studabaker, W.B., Krupa, S., Jayanty, R.K.M., Raymer, J.H., 2012. Measurement of polynuclear aromatic hydrocarbons (PAHs) in epiphytic lichens for receptor modeling in the Alberta Oil Sands Region (AOSR): a pilot study. In: Percy, Kevin (Ed.), Alberta Oil Sands: Energy, Industry and the Environment. Elsevier, Oxford, England, pp. 391–425.
Studabaker, W.B., Puckett, K.J., Percy, K.E., Landis, M.S., 2017. Determination of polycyclic aromatic hydrocarbons, dibenzothiophene, and alkylated homologs in the lichen *Hypogymnia physodes* by gas chromatography using single quadrupole mass spectrometry and time-of-flight mass spectrometry. J. Chromatogr. A 1492, 106–116.
U.S. Environmental Protection Agency, 2014a. EPA Positive Matrix Factorization (PMF) 5.0 Fundamentals & User Guide. Report No. EPA-600/R-14/108. Office of Research and Development, Washington, DC, USA.
U.S. Environmental Protection Agency, 2014b. SPECIATE Version 4.5 Database Development Documentation. Report No. EPA/600/R-16/294. Office of Research and Development, Washington, DC, USA.
Van der Wat, L., Forbes, P.B.C., 2015. Lichens as biomonitors for organic air pollutants. Trends Anal. Chem. 64, 165–172.
Wang, Z., Fingas, M.F., 2003. Development of oil hydrocarbon fingerprinting and identification techniques. Mar. Pollut. Bull. 47, 423–452.
Wang, Z.D., Fingas, M., Shu, Y.Y., Sigouin, L., Landriault, M., Lambert, P., Turpin, R., Campagna, P., Mullin, J., 1999. Quantitative characterization of PAHs in burn residue and soot samples and differentiation of pyrogenic PAHs from petrogenic PAHs - the 1994 mobile burn study. Environ. Sci. Technol. 33, 3100–3109.
Wang, Z., Yang, C., Kelly-Hooper, F., Hollebone, B.P., Peng, X., Brown, C.E., Landriault, M., Sun, J., Yang, Z., 2009. Forensic differentiation of biogenic organic compounds from petroleum hydrocarbons in biogenic and petrogenic compounds cross-contaminated soils and sediments. J. Chromatogr. A 1216, 1174–1191.
Wang, X., Chow, J.C., Kohl, S.D., Percy, K.E., Legge, A.H., Watson, J.G., 2015. Characterization of $PM_{2.5}$ and PM_{10} fugitive dust source profiles in the Athabasca Oil Sands Region. J. Air Waste Manage. Assoc. 65, 1421–1433.
Wang, X., Chow, J.C., Kohl, S.D., Percy, K.E., Legge, A.H., Watson, J.G., 2016. Real-world emission factors for Caterpillar 797B heavy haulers during mining operations. Particuology 28, 22–30.
Wentworth, G., Aklilu, Y.A., Landis, M.S., Hsu, Y.M., 2018. Impacts of a large boreal wildfire on ground level atmospheric concentrations of PAHs, VOCs and ozone. Atmos. Environ. 178, 19–30.
Wieder, R.K., Vile, M.A., Scott, K.D., Albright, C.M., McMillen, K.J., Vitt, D.H., Fenn, M.E., 2016. Differential effects of high atmospheric N and S deposition on bog plant/lichen tissue and porewater chemistry across the Athabasca Oil Sands Region. Environ. Sci. Technol. 50 (23), 12630–12640.
Yang, Z.Y., Yang, C., Wang, Z.D., Hollebone, B., Landriault, M., Brown, C.E., 2011. Oil fingerprinting analysis using commercial solid phase extraction (SPE) cartridge and gas chromatography–mass spectrometry (GC–MS). Anal. Methods 3, 628–635.
Yang, C., Zhang, G., Wang, Z.D., Yang, Z.Y., Hollebone, B., Landriault, M., Shah, K., Brown, C.E., 2014. Development of a methodology for accurate quantitation of alkylated polycyclic aromatic hydrocarbons in petroleum and oil contaminated environmental samples. Anal. Methods 6, 7760–7771.
Zhang, Y., Shotyk, W., Zaccone, C., Noernberg, T., Pellerier, R., Bicalho, B., Froese, D.G., Davies, L., Martin, J.W., 2016. Airborne petcoke dust is a major source of polycyclic aromatic hydrocarbons in the Athabasca Oil Sands Region. Environ. Sci. Technol. 50, 1711–1720.